

Nelfinavir and its active metabolite M8 are partial agonists and competitive antagonists of the human pregnane X receptor

Oliver Burk, Thales Kronenberger¹, Oliver Keminer, Serene M. L. Lee, Tobias S. Schiergens, Matthias Schwab, Björn Windshügel

Dr. Margarete Fischer-Bosch-Institute of Clinical Pharmacology, Stuttgart, and University of Tübingen, Tübingen, Germany (O.B., M.S.); Fraunhofer Institute for Molecular Biology and Applied Ecology IME, ScreeningPort, Hamburg, Germany (T.K., O.K., B.W.); Biobank of the Department of General, Visceral, and Transplantation Surgery, University Hospital LMU Munich, Munich, Germany (S.M.L.L., T.S.S.); Departments of Clinical Pharmacology, and Pharmacy and Biochemistry, University of Tübingen, Tübingen, Germany (M.S.); and Institute for Biochemistry and Molecular Biology, Department of Chemistry, Universität Hamburg, Germany (B.W.)

Running title: Nelfinavir and PXR

Address correspondence to:

Oliver Burk, Dr. Margarete Fischer-Bosch-Institute of Clinical Pharmacology, Auerbachstrasse 112,
70376 Stuttgart, Germany. Phone +49 711 8101-5091, Fax +49 711 859295, E-mail oliver.burk@ikp-stuttgart.de

or

Björn Windshügel, Fraunhofer Institute for Molecular Biology and Applied Ecology IME,
ScreeningPort, Schnackenburgallee 114, 22525 Hamburg, Germany. Phone +49 40 303764-286, Fax
+49 40 303764 100, E-mail bjoern.windshuegel@ime.fraunhofer.de

Number of text pages: 37

Number of Tables: 0

Number of Figures: 7

Number of References: 59

Number of words in the Abstract: 250

Number of words in the Introduction: 748

Number of words in the Discussion: 1498

Abbreviations: AD, activation domain; CAR, constitutive androstane receptor; CDK, cyclin-dependent protein kinase; CYP, cytochrome P450; DBD, DNA binding domain; FBS, fetal bovine serum; FXR, farnesoid X receptor; LBD, ligand binding domain; LBP, ligand binding pocket; LXR,

liver X receptor; MED1, mediator complex subunit 1; NCOA, nuclear receptor co-activator; NCOR2, nuclear receptor co-repressor 2; PPAR, peroxisome proliferator-activated receptor; PXR, pregnane X receptor; RID, receptor interaction domain; THR, thyroid hormone receptor; TR-FRET, time-resolved fluorescence resonance energy transfer; VDR, vitamin D receptor

Abstract

The HIV protease inhibitor nelfinavir is currently being analyzed for repurposing as an anticancer drug for many different cancers, as it exerts manifold off-target protein interactions, finally resulting in cancer cell death. Xenosensing pregnane X receptor (PXR), which also participates in the control of cancer cell proliferation and apoptosis, was previously shown to be activated by nelfinavir, however the exact molecular mechanism is still unknown. The present study addresses the effects of nelfinavir and its major and pharmacologically active metabolite nelfinavir hydroxy-tert-butylamide (M8) on PXR to elucidate the underlying molecular mechanism. Molecular docking suggested direct binding to the PXR ligand binding domain, which was confirmed experimentally by limited proteolytic digestion and competitive ligand binding assays. Concentration response analyses using cellular transactivation assays identified nelfinavir and M8 as partial agonists with EC_{50} values of 0.9 μ M and 7.3 μ M, and competitive antagonists of rifampin-dependent induction with IC_{50} values of 7.5 μ M and 25.3 μ M, respectively. Antagonism exclusively resulted from binding into the PXR ligand binding pocket. Impaired co-activator recruitment by nelfinavir, as compared to the full agonist rifampin, proved to be the underlying mechanism of both effects on PXR. Physiological relevance of nelfinavir-dependent modulation of PXR activity was investigated in respectively treated primary human hepatocytes, which showed differential induction of PXR target genes and antagonism of rifampin-induced ABCB1 and CYP3A4 gene expression. In conclusion, we elucidated here the molecular mechanism of nelfinavir interaction with PXR. It is hypothesized that modulation of PXR activity may impact on the anticancer effects of nelfinavir.

Significance Statement:

Nelfinavir, which is being investigated for repurposing as an anticancer medication, is shown here to directly bind to human PXR and thereby act as a partial agonist and competitive antagonist. Its major metabolite M8 exerts the same effects, which are based on impaired co-activator recruitment. Nelfinavir anticancer activity may involve modulation of PXR, which itself is discussed as a therapeutic target in cancer therapy and for the reversal of chemoresistance.

Introduction

The HIV protease inhibitor nelfinavir is no longer commonly used in modern anti-retroviral therapy of AIDS, due to the introduction of more efficacious medications. However, it is a promising candidate for repurposing as an anticancer drug for many different cancers (for review see Shim and Liu, 2014; Bhattarai et al., 2016). This is because of the manifold off-target interactions of nelfinavir, which not only targets HIV protease, but also inhibits, among others, the activities of 20S proteasome (Gupta et al., 2007), cyclin-dependent protein kinase (CDK) 2 (Jiang et al., 2007), site-2-protease (Guan et al., 2011) and heat shock protein 90 (Shim et al., 2012). Proteome-wide in silico analysis of nelfinavir potential off-target interactions suggested the interaction with and possible inhibition of multiple protein kinases (Xie et al., 2011). Due to these interactions, nelfinavir results in diverse effects on cancer cells, such as inhibition of the PI3K-AKT-mTOR pathway and induction of endoplasmic reticulum stress, which finally lead to cell death by cell cycle arrest, triggering of the unfolded protein response, apoptosis and autophagy (Koltai, 2015). The major and anti-virally equipotent metabolite hydroxy-*tert*-butylamide (Zhang et al., 2001), also designated as M8, demonstrated in vitro antitumor activity comparable to that of the parent compound (Guan et al., 2011). M8 likely contributes to total nelfinavir antiviral and anticancer activity, as its concentrations in human plasma reach up to one third of those of nelfinavir (Zhang et al., 2001).

The nuclear receptor pregnane X receptor (PXR, NR1I2) is one of the many targets of nelfinavir. In response to xenobiotics, PXR transcriptionally regulates the expression of cytochrome P450 drug metabolizing enzymes and drug transporters such as CYP3A4 and P-glycoprotein (MDR1/ABCB1). As nelfinavir-dependent induction of the respective genes and proteins was demonstrated in rats (Huang et al., 2001), primary human hepatocytes (Dixit et al., 2007; Liu et al., 2012) and the human colorectal adenocarcinoma cell lines LS174T and LS180 (Huang et al., 2001; Gupta et al., 2008), it is assumed that nelfinavir activates PXR. However, inconsistent results were obtained when analyzing nelfinavir-dependent PXR activation using cellular transactivation assays. While nelfinavir did not activate PXR in a one-hybrid reporter gene assay in monkey kidney fibroblast CV-1 cells (Dussault et al., 2001), it induced PXR-dependent activation of CYP3A4 and CYP2B6 promoter reporter genes in

human hepatocellular carcinoma HepG2 cells (Svärd et al., 2010; Lynch et al., 2015). In contrast, knockdown experiments in LS180 cells clearly attributed the nelfinavir-dependent induction of CYP3A4 and ABCB1 gene expression to PXR (Gupta et al., 2008). However, as former work had also demonstrated that nelfinavir neither bound to the PXR ligand binding domain in vitro, nor recruited co-activator MED1 to PXR in a mammalian two-hybrid assay (Dussault et al., 2001), the molecular mechanism of nelfinavir-dependent PXR activation remains obscure. As mentioned above, nelfinavir was shown to inhibit CDK2 activity and is further supposed to also inhibit CDK5 and cAMP-dependent protein kinase (Xie et al., 2011), which have all been shown to phosphorylate PXR in vitro and thereby inhibit its transactivation activity (for a review, see Mackowiak and Wang, 2016). Altogether, published data do not provide evidence for direct binding of nelfinavir to PXR and are consistent with a putative indirect activation mechanism of the drug, which may rely on the inhibition of inhibitory protein kinases.

Given the current efforts to repurpose nelfinavir as an anticancer drug, it is of interest that PXR is discussed as a therapeutic target in anticancer therapy. Depending on the cancer entity, PXR activation may either result in tumor progression and promote chemoresistance or suppress cancer cell growth (Pondugula et al., 2016; Xing et al., 2020). In the latter case, PXR activation may contribute to nelfinavir's anticancer activity. A thorough understanding of how exactly the drug affects PXR activity will promote our knowledge on the potential of nelfinavir as an anticancer drug.

We aim here to elucidate the molecular mechanism of nelfinavir-dependent activation of PXR and to investigate the PXR interaction properties of the pharmacologically equipotent major metabolite M8. By using a combination of biochemical and cellular assays, as well as in silico molecular modelling, it is shown that nelfinavir and M8 bind to human PXR and act both as partial agonists and competitive antagonists. Impaired recruitment of co-activators mainly accounts for these properties. Studies in primary human hepatocytes demonstrate the physiological relevance of nelfinavir's agonism and antagonism of PXR; however, nelfinavir exhibits differential induction of PXR target genes. The chemical structure of nelfinavir may thus represent a suitable starting point for the development of PXR selective modulators.

Materials and Methods

Chemicals and biological reagents

Rifampin was purchased from Merck Chemicals (Darmstadt, Germany); Tocris Bioscience (Bristol, UK) provided T0901317, GW4064 and SR12813; nelfinavir and nelfinavir hydroxy-*tert*-butylamide (M8) were purchased from Toronto Research Chemicals (North York, Canada); DMSO, GW3965, triiodo-L-thyronine, and 1 α ,25-dihydroxyvitamin D3 were provided by Sigma-Aldrich (Munich, Germany); rosiglitazone and CITCO were purchased from Sellekchem (Houston, TX) and ENZO Life Sciences (Lörrach, Germany), respectively. SPA70 was provided by Axon Medchem (Groningen, The Netherlands). Cell culture medium and supplements were obtained from Life Technologies (Darmstadt, Germany).

Plasmids

Eukaryotic expression plasmids encoding full-length human nuclear receptors PXR (Geick et al., 2001), constitutive androstane receptor (CAR) 1 (Burk et al. 2002) and CAR3 (Arnold et al. 2004), thyroid hormone receptor (THR) α 1, THR β 1, vitamin D receptor (VDR) (Burk et al., 2005), liver X receptor (LXR) α and LXR β (Piedade et al. 2015) have all been described. Expression plasmids encoding the human small PXR variant, which consists of the ligand binding domain (amino acids 113-434) only (Jeske et al., 2017), and PXR mutant S208W/S247W/C284W (Burk et al., 2018) have already been described. T. Tanaka kindly provided the human peroxisome proliferator-activated receptor (PPAR) γ 1 expression plasmid (Tachibana et al., 2005). Farnesoid X receptor (FXR) α 2 expression plasmid was constructed by cloning the respective open reading frame, amplified by PCR from the cDNA of primary human hepatocytes using appropriate primers, into expression vector pcDNA3 (Thermo Fisher Scientific Invitrogen, Carlsbad, CA). The 5' upstream primer additionally introduced an optimized Kozak consensus sequence. Sequencing identified a FXR clone lacking the 12 bp insertion, which encodes amino acids MYTG, i.e. FXR α 2.

Expression plasmids encoding fusion proteins of the GAL4-DNA binding domain (DBD) and the receptor interaction domains (RID) of nuclear receptor co-activator (NCOA) 1, residues 583-783),

NCOA2 (residues 583-779), mediator complex subunit 1 (MED1, residues 527-774) (Arnold et al. 2004) and nuclear receptor co-repressor (NCOR) 2, (residues 1109-1330) or helix 1 part of the ligand binding domain (LBD) of PXR (residues 132-188) as well as expression plasmids encoding fusion proteins of the VP16 activation domain (AD) and the whole or part of the PXR-LBD (residues 108-434 and 189-434, respectively) (Burk et al., 2005) have been described. The expression plasmid encoding the fusion protein of GAL4-DBD with PXR-LBD (residues 108-434) was constructed by subcloning the insert of pVP16-AD/PXR-LBD(108-434) into pM (Takara Bio Clontech, Mountain View, CA).

Firefly luciferase reporter gene plasmids have previously been described: CYP3A4 enhancer/promoter reporter gene plasmid pGL4-CYP3A4(7830/Δ7208-364) (Burk et al., 2018); CYP2B6 enhancer/promoter reporter gene plasmid pB-1.6k/PB/XREM was provided by H. Wang (Wang et al. 2003); reporter gene plasmid comprising a dimer of the MDR1-DR4(I) motif (Geick et al. 2001); pGL3(DR3)₃Tk (Hustert et al., 2001); plasmid PPRE X3 Tk-luc (Addgene plasmid #1015) was provided by B. Spiegelman (Forman et al., 1995); reporter gene plasmid containing a dimer of the consensus nuclear receptor inverted repeat (IR) 1 motif (Piedade et al. 2015); GAL4-dependent reporter gene plasmid pGL3-G5 (Arnold et al. 2004). With the exception of the CYP3A4 and CYP2B6 reporters and pGL3-G5, the other reporter gene plasmids harbor the thymidine kinase (Tk) minimal promoter. The *Renilla* luciferase expression plasmid pGL4.75[hRluc/CMV] (Promega, Madison, WI) has been used.

Molecular docking

Three-dimensional coordinates for nelfinavir and its metabolite M8 were generated within MOE version 2019.01.02 (Chemical Computing Group Inc., Montreal, Canada). All PXR X-ray crystal structures were downloaded from the Protein Data Bank (Berman et al., 2000). Based on a structural analysis of all available PXR X-ray crystal structures using PROCHECK and ProSa (Laskowski et al, 1993; Sippl, 1993), PDB IDs 1M13, 1NRL, and 2O9I were selected for docking. For 1M13 two

separate structures with different alternate atoms for Cys284 were generated, and both chains of 1NRL and 2O9I were selected, resulting in an ensemble of 6 LBD structures. The mutation C284S in 2O9I was mutated back into the wildtype residue using MOE and solvent atoms were removed. All structures were superposed on C α atoms of amino acids lining the ligand-binding pocket (LBP). Protein structures were prepared using Protonate3D in MOE and energy minimized (Amber10:EHT force field with R-Field implicit solvation model) using a three-step procedure (C α atoms, backbone, all atoms) with a tether of 0.5 and a RMS gradient of 5. Alternative ligand-binding on the LBD surface sites were identified by applying Site Finder in MOE. Compounds were docked using GOLD version 5.8.1 (Cambridge Crystallographic Data Centre, Cambridge, UK). The docking search space for the LBP was defined by a sphere of 13 Å radius centered on coordinates of atom C27 of the ligand hyperforin (PDB ID 1M13), while for the AF-2 site a sphere of 10 Å radius centered on atom CD2 of Leu670 (PDB ID 1NRL, chain C) was used. The docking search space for the alternative sites were defined by the amino acids lining the pockets. For each compound 100 docking runs were conducted. The early termination option was switched off.

Limited proteolytic digestion

Radiolabeled PXR-LBD protein (residues 113-434) was synthesized in vitro using the TNT T7 Quick Coupled Transcription/Translation System (Promega) as recommended by the manufacturer. Briefly, 50 µl reactions were set up with 40 µl TNT T7 Quick Master Mix, 20 µCi ³⁵S-methionine (specific activity >1000 Ci/mmol; Hartmann Analytic, Braunschweig, Germany) and 1 µg of the small PXR expression plasmid. 5 µl aliquots thereof were pre-incubated with compounds or solvent DMSO for 30 min and then subjected to proteolytic digestion with trypsin for 10 min, as described (Jeske et al., 2017). Reactions were separated on 12% SDS polyacrylamide gels, which were subsequently stained with Coomassie, dried and exposed to BAS-IP MS 2325 imaging plates (Fuji, Kanagawa, Japan). Input PXR-LBD protein and protected proteolytic fragments were detected by scanning the imaging plates with the CR35 Bio radioluminography laser scanner (Raytest, Straubenhardt, Germany) and

quantified using AIDA software version 4.50.010 (Raytest). Each independent experiment was performed in technical single replicates.

Competitive ligand binding

Ligand binding to PXR was investigated using the Lanthascreen® TR-FRET PXR (SXR) competitive binding assay kit (PV4839, lot 2109118, Thermo Fisher Scientific, Waltham, MA). All assay steps and the detection were carried out according to the protocol and microplate reader-specific guidelines of the manufacturer. In brief, the assay was performed in a volume of 20 µl per well of 384-well black, non-binding, low volume plates (Corning Life Sciences, Amsterdam, The Netherlands) with 2.5 nM GST-PXR-LBD, 40 nM Fluormone™ PXR Green and 10 nM terbium-labeled anti-GST antibody. Positive control (SR12813) and test compounds nelfinavir and M8 were added at concentrations ranging from 0.5 nM to 30 µM. Reactions were incubated for 60 min at room temperature in the dark. The fluorescent emissions were measured on an Infinite M1000 multimode microplate reader (Tecan, Männedorf, Switzerland) at 486 nm and 515 nm. All measurements were optimized using maximum signal control reactions (100 µs lag time, 200 µs integration, flash mode 2 [100 Hz, ~8 joule]). The FRET ratio was calculated by dividing the emission signal at 515 nm by that at 486 nm. 2% DMSO was used as the negative control (0% relative binding) and 30 µM SR-12813 as the positive control (100% relative binding). The data were expressed as relative binding (%) [relative binding (%) = 100% × (DMSO FRET ratio – compound FRET ratio)/(DMSO FRET ratio - 30 µM SR12813 FRET ratio)], according to Dong et al. (2010).

Cell culture

HepG2 cells (HB-8065, lot number 58341723, ATCC, Manassas, VA) and H-P cells, which represent a HepG2 cell clone stably overexpressing human PXR (Bitter et al., 2015) were cultivated in minimal essential medium, supplemented with 10 % fetal bovine serum (FBS), 2 mM L-glutamine, 100 U/ml

penicillin and 0.1 mg/ml streptomycin. In drug treatments, dextran-coated charcoal-stripped FBS replaced regular FBS. Both cell lines were routinely checked for contamination with mycoplasma by PCR (VenorGeM Classic, Minerva Biolabs, Berlin, Germany).

Concentration response analyses

Transient transfections of H-P cells were set up according to the batch protocol for jetPEI[®] (Polyplus, Illkirch, France). Transfected cells were seeded in 96-well Cell+ flat-bottom microplates (Sarstedt, Nümbrecht, Germany) using per well 250 µl of a suspension, consisting of 200 µl H-P cells (4×10^4 cells) and 50 µl transfection mixture, containing 0.3 µg CYP3A4 reporter gene plasmid, 0.01 µg pGL4.75[hRluc/CMV]) and 0.6 µl jetPEI[®] transfection reagent in 150 mM NaCl. 24 h after transfection, cells were treated with varying concentrations of chemicals ranging from 0.03 µM to 10 µM (nelfinavir and M8) or 30 µM (rifampin), in the presence or absence of fixed concentrations of competing ligands, for another 24 h in a volume of 100 µl. Then, culture medium was removed and cells were lysed with 50 µl of 1x passive lysis buffer (Promega). Firefly and *Renilla* luciferase assays were performed separately with 10 µl lysate each, in white opaque 96-well microplates (OptiPlate-96, Perkin-Elmer), by adding 150 µl or 100 µl of respective assay solutions, which have been described previously (Geick et al. 2001; Piedade et al. 2015). Luminescence was measured after 10 min incubation at constant shaking with the 2300 EnSpire multimode plate reader (Perkin Elmer, Rodgau, Germany) for 0.1 sec. Concentration response experiments were done 5 to 7 times independently, each in technical triplicates.

Nuclear receptor specificity, mammalian two-hybrid and mutant PXR assays

Transient transfections were performed in 24-well plates with 1.5×10^5 HepG2 cells per well, seeded the day before, using per well 1 µl jetPRIME[®] transfection reagent (Polyplus) and a plasmid DNA mixture consisting of 0.04 µg of the respective nuclear receptor (NR) expression plasmids, 0.3 µg

corresponding firefly luciferase reporter gene constructs, 0.005 µg pGL4.75[hRluc/CMV], filled up with pUC18 to 0.5 µg. The following reporter gene plasmids were used for the NR specificity tests: CYP3A4 reporter (PXR) and CYP2B6 reporter (CAR1, CAR3); MDR1-DR4 reporter (LXRα, LXRβ, TRα1, TRβ1), DR3 reporter (VDR); PPRE X3 Tk-luc (PPARγ1); consensus IR1 reporter (FXRα2). In the antagonist mode, the following prototypical agonist were further utilized; 10 µM rifampin (PXR), 10 µM CITCO (CAR3), 2 µM GW3965 (LXRα, LXRβ), 1 µM triiodo-L-thyronine (TRα1, TRβ1), 0.1 µM 1α,25-dihydroxyvitamin D3 (VDR), 1 µM rosiglitazone (PPARγ1), and 1 µM GW4064 (FXRα2). Transfections for mammalian two-hybrid PXR co-repressor, co-activator and LBD assembly assays were set up similarly, using the plasmids specified in the legend of Fig. 6. In mutant PXR assays, respective PXR expression plasmids were combined with the CYP3A4 reporter as described above. 20 h after transfection, cells were treated with chemicals for another 24 h. Cell lysis and reporter gene assays were performed as described above. All transfections were done 4 to 5 times independently, each in technical triplicates, and with at least two different preparations of plasmids.

Human liver tissue samples and primary human hepatocytes

Double-coded human liver samples and corresponding data used in this study were provided by the Biobank of the Department of General, Visceral and Transplantation Surgery in Ludwig-Maximilians University (LMU). This Biobank operates under the administration of the Human Tissue and Cell Research (HTCR) Foundation. The framework of HTCR Foundation (Thasler et al. 2003), which includes obtaining written informed consent from all donors, has been approved by the ethics commission of the Faculty of Medicine at the LMU (approval number 025-12) as well as the Bavarian State Medical Association (approval number 11142) in Germany. Experimental procedures were performed in accordance with the Declaration of Helsinki. Donor data are shown in Supplemental Table S1. Primary human hepatocytes were isolated by the Biobank using a two-step collagenase perfusion technique with modifications (Lee et al. 2013). The cells were cultivated and treated with chemicals as described before (Jeske et al. 2017).

RNA isolation and reverse transcription quantitative real-time PCR analysis

Total RNA was isolated using the NucleoSpin RNA kit (Machery-Nagel, Düren, Germany), including on-column DNase I digest. RNA integrity was analyzed by formaldehyde-agarose gel electrophoresis. cDNA was synthesized as described previously (Jeske et al. 2017).

Relative quantification analyses ($\Delta\Delta C_t$) were performed in technical triplicates by TaqMan RT-qPCR using the BioMark HD system and 48.48 Dynamic Array or Flex Six Gene Expression Integrated Fluidic Circuits (Fluidigm, South San Francisco, CA), as described previously (Jeske et al., 2017). The following TaqMan gene expression assays (Life Technologies) were used: Hs00184500_m1 (ABCB1), Hs01546975_gH (AKR1B10), Hs00946140_g1 (CYP2C8), Hs00604506_m1 (CYP3A4), Hs01005622_m1 (FASN), Hs00378308_m1 (SMPDL3A), Hs99999902_m1 (RPLP0). The CYP2B6, EPHX1 and UGT1A3 assays have been described previously (Burk et al. 2005; Hoffart et al. 2012; Riedmaier et al. 2010). Data were analyzed as described before (Jeske et al. 2017) and gene expression levels were normalized to corresponding 18S rRNA levels, as determined using the 18S rRNA assay previously described (Hoffart et al. 2012). Serial dilutions of respective linearized cDNA plasmids, which were treated just as cDNA samples, were used to determine linearity of the assays (between 375,000 and 37.5 copies).

Experimental design and data analyses

All experiments were done in an exploratory manner. Thus, p-values have to be interpreted as descriptive only. The decision to perform five independent experiments (except competitive PXR binding and hepatocyte experiments) was made prior to their execution, based on the level of variation observed in previous work. In Figure 4A,C,D, the number of independent experiments for controls (RIF, without NFV, or without M8) exceeds five, due to technical reasons. To avoid systematic errors due to timing and/or positioning in limited proteolytic digestion and transfection

experiments, the sequence of chemical treatment of cells and measurement of samples was randomized for independent experiments.

Experimental data are shown in scatter plots with means \pm standard deviation (S.D.) or medians with interquartile ranges of at least five independent experiments. Numbers of independent experiments are presented in the respective figure legends. Medians were used only with primary human hepatocytes, as independent experiments were performed here with cultures from different donors. Statistical comparisons were performed with repeated measures one-way or two-way analysis of variance (ANOVA) or Friedman test, using respective post-hoc tests for multiple comparisons against specified controls, as recommended by the analysis software and described in the figure legends. Comparisons to a hypothetical value were performed with one sample *t* test or Wilcoxon signed rank test for means or medians, respectively. Pairwise comparisons of medians were performed with Wilcoxon matched-pairs signed rank test. EC₅₀ and IC₅₀ values were determined by non-linear fit of concentration response using the equation for sigmoidal dose response (log agonist or log inhibitor vs. response (three parameters)). All calculations were done with GraphPad Prism 8.4.2 (GraphPad Software, La Jolla, CA, USA).

Results

Nelfinavir and its metabolite M8 modulate the activities of PXR and further nuclear receptors

Expression of drug metabolizing enzymes and transporters is not exclusively induced via PXR, but also by further ligand-activated nuclear receptors (for a review see Pascussi et al., 2003; Prakash et al., 2015). Thus, we investigated whether nelfinavir and its metabolite M8 (Fig. 1A) modulate the activities of respectively selected nuclear receptors using the corresponding promoter reporter gene assays in agonist (Fig. 1B) and antagonist (Fig. 1C) modes. To determine the applicable concentration, the effects of increasing concentrations of the compounds on viability of HepG2 cells were analyzed. Supplemental Figure S1 shows for both compounds that concentrations exceeding 10 μ M resulted in HepG2 viability of less than 80%. Thus, single concentration of 10 μ M of nelfinavir and M8 was selected for starting analyses. In accordance with published results (Sv rd et al., 2010; Lynch et al., 2015), nelfinavir induced PXR activity by 3.7-fold (95% CI 3.1- to 4.3-fold), while inhibiting the constitutive activity of CAR1 by 60% (95% CI 51-72%). In addition, FXR 2 was also activated 2.0-fold (95% CI 1.7- to 2.3-fold) by nelfinavir. M8 selectively induced PXR activity by 5.1-fold (95% CI 4.5- to 5.7-fold) (Fig. 1B). The 20% reduction of basal PPAR 1 activity may indicate antagonism of M8. Figure 1C shows that nelfinavir antagonized rifampin-dependent PXR activity by 35% (95% CI 19-51%), while M8 demonstrated 50% (95% CI 24-77%) inhibition. Ligand-activated VDR was inhibited by 15% or 45% in the presence of nelfinavir or M8, respectively, while the activity of GW4064-induced FXR 2 was reduced by 17% or 40%, respectively. In addition, the activities of ligand-activated CAR3, LXR  and PPAR 1 were all reduced approximately by 30% in the presence of M8.

To corroborate the above-described effects of nelfinavir and M8 on nuclear receptors besides PXR, respective concentration response analyses were conducted. Nelfinavir-dependent inhibition of CAR1 and activation of FXR 2 were confirmed unequivocally (Suppl. Fig. S2A, E). However, the effects on the other nuclear receptors, which mainly consisted of slight inhibition of agonist-induced receptor activities by M8, were exclusively obtained with 10 μ M. Concentration-dependent effects, as with CAR1 and FXR 2, were not observed (Suppl. Fig. S2B-D,F-H). Given the sharp decline in viability

of HepG2 between 10 μ M and 30 μ M of M8 (Suppl. Fig. S1), it cannot be excluded that the effects observed with 10 μ M M8 stemmed from partial cytotoxicity. In conclusion, nelfinavir and its metabolite M8 not only activated PXR, but also antagonized the ligand-activated receptor. Additionally, nelfinavir inhibited CAR1 and activated FXR α 2, while effects on some other nuclear receptors, especially by M8, have to be regarded as uncertain due to the possibility of partial cytotoxicity.

Direct binding of nelfinavir and M8 to PXR

As mentioned above, activation of PXR by nelfinavir and M8 may be explained theoretically by the inhibition of inhibitory protein kinases. However, the antagonistic effects on rifampin-induced PXR activity identified here call for a different explanation. Thus, direct binding of the compounds to PXR was re-investigated. First, we addressed binding by *in silico* molecular docking of nelfinavir and M8 into different potential binding sites. An ensemble docking approach was chosen, by which nelfinavir and M8 were flexibly docked into the LBP and AF-2 groove of six different PXR X-ray crystal structures. Docking scores of the top-ranked poses of both compounds were similar for the LBP (107.4 for nelfinavir vs. 110.4 for M8) and thus do not indicate a preferred binding of either nelfinavir or M8 over each other. Docking scores for the AF-2 groove were substantially lower (nelfinavir: 84.2; M8: 85.4), indicating a preference of both compounds for the LBP (Suppl. Table S2). In order to evaluate binding of nelfinavir and M8 to alternative sites on the LBD, an *in silico* approach for pocket detection was employed (Fig. 2A). Only pockets with either a size of >50 alpha spheres or a calculated propensity for ligand binding >1 were considered, resulting in a total of eight potential alternative binding sites (Figure 2A, Suppl. Table S2) into which nelfinavir and M8 were docked. Docking scores for all alternative sites were substantially lower compared to the scores obtained for the LBP (63.7-82.9). Thus, the further analysis was continued only for nelfinavir and M8 docking poses within the LBP. Clustering of the docking poses revealed the ten top-ranked poses (RMSD cut-off 1.5 Å) of nelfinavir to appear in two clusters and two single conformations (Suppl. Table S3). Six of the ten best-scored docking poses belong to the same cluster. In contrast, the ten top-ranked

conformations for M8 grouped into five clusters and one single conformation. The visualization of the top-ranked docking poses of each cluster showed that M8 samples a considerably larger conformational space in the LBP compared to nelfinavir (Fig. 2B,C). This suggests the preference of nelfinavir for a specific binding mode within the LBP compared to M8.

The *in silico* prediction of binding was checked experimentally with the limited proteolytic digestion assay. Figure 3A shows that nelfinavir, as well as its metabolite M8, result in concentration-dependent increase in protection of three main proteolytic fragments of the 36 kDa PXR-LBD protein from trypsin digestion. At the highest concentration, nelfinavir showed 5.3-fold increase (95% CI 3.7- to 7.0-fold), while M8 showed 5.4-fold increase (95% CI 4.5- to 6.2-fold). Similarly, the high affinity PXR ligand T0901317 demonstrated 5.0-fold increase (95% CI 4.3- to 5.7-fold). T0901317 protected the same main proteolytic fragments, although at varying extent. While nelfinavir and M8 only weakly protected the 26 kDa fragment, T0901317 efficiently protected all three, suggesting that PXR binding of nelfinavir and M8 may have resulted in a LBD conformational change different from that generated by binding of T0901317. To further confirm direct binding to PXR, a competitive PXR binding assay was deployed (Fig. 3B). EC₅₀ value of % relative binding of positive control SR12813 was determined as 45.6 nM (95% CI 22.7-94.1 nM), which is in line with published data (Dong et al., 2010). Nelfinavir and M8 also demonstrated PXR binding in this assay with EC₅₀ values of 89.0 nM (95% CI 48.2-167 nM) and 51.1 nM (95% CI 18.7-148 nM), respectively. In summary, these data provide evidence for direct binding of nelfinavir and M8 to the PXR-LBD.

Nelfinavir and M8 are partial agonists of PXR, which also act as competitive antagonists

Having established ligand binding to PXR, further characterization of the respective activation and inhibition properties of nelfinavir and M8 called for cellular concentration response analyses. Respective analyses were performed with H-P cells, a HepG2 clone stably expressing PXR (Bitter et al., 2015). Similar as parental HepG2 cells, H-P showed decreased viability at compound concentrations exceeding 10 μ M, however they were not as sensitive towards M8 as HepG2 (Suppl. Fig S1). Figure 4A shows that the agonist efficacies of nelfinavir and M8 were reduced, if compared

to rifampin. At 10 μM , the two compounds exhibited only 30-40% of the activity seen by the same concentration of rifampin, thereby indicating partial agonism. Keeping in mind that the M8 concentration response curve did not yet approximate plateau, nelfinavir demonstrated EC_{50} of 0.9 μM (95% CI 0.58-1.3 μM), while M8 showed reduced potency with EC_{50} of 7.5 μM (95% CI 4.4-14.9 μM). Using the same assay, rifampin EC_{50} of 2.4 μM (95% CI 1.6-3.6 μM) proved to be elevated, compared to previously reported EC_{50} values of 1.3 μM and 1.8 μM (Lin et al., 2008; Hoffart et al., 2012). Partial agonism was also observed for nelfinavir-dependent activation of a GAL4-DBD/PXR-LBD fusion protein (Suppl. Fig. S3). Co-treatment with the specific PXR antagonist SPA70 (Lin et al., 2017) almost completely suppressed the reporter activation by nelfinavir and M8 (Fig. 4B), thereby testifying PXR-dependency. Competitive antagonism of the compounds was observed, when rifampin concentration response curves were established in the presence of increasing concentrations of nelfinavir (Fig. 4C) or M8 (Fig. 4D). In both cases, rifampin concentration response curves were shifted to the right and respective EC_{50} values increased with elevated concentrations of the antagonistic compounds (Suppl. Table S4). Analysis of the increase in rifampin EC_{50} values revealed statistical significance only for 10 μM nelfinavir. However, a respective trend was observed for 3 μM nelfinavir and 10 μM M8 (Fig. 4E). IC_{50} values of nelfinavir and M8 antagonism were determined for the inhibition of PXR activation by 10 μM rifampin (Fig. 4F). With IC_{50} of 7.3 μM (95% CI 5.0-11.0 μM), nelfinavir proved to be the more potent antagonist when compared to M8, with IC_{50} of 25.3 μM (95% CI 16.1-47.2 μM). Nelfinavir further proved to antagonize PXR activation by the high affinity ligand T0901317 (Suppl. Fig. S4). As nelfinavir and M8 comparably affected PXR, and cytotoxicity of M8 was more pronounced, further investigations were performed only with the parent drug.

Competitive antagonism of nelfinavir exclusively depends on binding into the PXR ligand binding pocket

As the concentration of nelfinavir had to be restricted to 10 μM , additional allosteric antagonism at higher concentrations, as observed for the PXR mixed competitive/non-competitive allosteric

antagonist pimecrolimus (Burk et al., 2018), may have remained undetected. Thus, we investigated the ability of nelfinavir to inhibit the constitutive activity of a PXR mutant with the LBP filled with bulky amino acid residues. Such a mutant is no longer activated by agonists, as these cannot bind into the LBP (Wang et al., 2008), but its constitutive activity can be antagonized by compounds exclusively or additionally binding outside of the LBP, *e.g.* coumestrol, pazopanib or pimecrolimus (Wang et al., 2008; Burk et al., 2018). Accordingly, nelfinavir showed activation of wild type PXR but not of the LBP-filled triple mutant S208W/S247W/C284W, which is similar to the prototypical PXR agonist rifampin. Nelfinavir, which inhibited the rifampin-dependent activation of wild type PXR by 54% (95% CI 29-80%), did not antagonize the high constitutive activity of the mutant (Fig. 5), thereby indicating that it has to bind to the LBP to exhibit its inhibitory effect.

Impaired co-activator recruitment accounts for the effects of nelfinavir on PXR activation

To characterize the functional consequences of nelfinavir interaction with PXR, cellular mammalian two-hybrid assays were performed, which address ligand-dependent LBD assembly, co-repressor release and co-activator recruitment. In clear contrast to the partial agonism of nelfinavir in the CYP3A4 enhancer/promoter reporter gene assay (as shown in Fig. 4A), the drug induced the PXR-LBD assembly more strongly (mean increase by 70%, 95% CI 19-120%) than rifampin (Fig. 6A). The constitutive interaction of PXR with co-repressor NCOR2 in the absence of ligand was diminished by nelfinavir to a similar extent as by rifampin (Fig. 6B). In the established sequence of events during nuclear receptor activation, recruitment of co-activators follows the ligand-dependent release of co-repressors. While rifampin induced the interaction of PXR with co-activators NCOA1, NCOA2 and MED1 by 8-fold (95% CI 4.6- to 12.2-fold), 9.3-fold (95% CI 7.3- to 11.3-fold) and 4.6-fold (95% CI 3.9- to 5.4-fold), respectively, nelfinavir demonstrated impaired recruitment for all co-activators, which have been tested (Fig. 6C-E). Furthermore, nelfinavir reduced the rifampin-dependent recruitment of NCOA1 to 3.2-fold (95% CI 1.8- to 4.6-fold) in co-treatment (Fig. 6C). Similar effects were observed with NCOA2 (4.1-fold, 95% CI 3.5- to 4.7-fold) (Fig. 6D) and MED1 (2.2-fold; 95% CI 2.0- to 2.4-fold) (Fig. 6E). Taken together, these data indicate that the partial agonism and

competitive antagonism of nelfinavir in PXR activation depend on the impaired recruitment of co-activators. Co-repressor release and intramolecular conformational changes in response to ligand binding, the latter as described by the LBD assembly assay, are not compromised.

Nelfinavir differentially induces PXR target genes in primary human hepatocytes and antagonizes rifampin induction

Given the weak activation of PXR by nelfinavir in reporter gene assays, the question arises, to which extent the compound may be able to induce the expression of endogenous PXR target genes. Primary human hepatocytes, which were treated with nelfinavir, demonstrated induction of only a subset of selected PXR-regulated genes, as compared to treatment with rifampin. Cytochrome P450 genes as CYP2B6, CYP2C8 and CYP3A4, which proved to be highly inducible by rifampin, also demonstrated induction by nelfinavir. Nelfinavir further induced the expression of EPHX1 and UGT1A3. However, genes such as ABCB1, AKR1B10, FASN or SMPDL3A, which showed weak to moderate induction by rifampin, were not induced by nelfinavir (Fig. 7A). Among the genes induced by both compounds, UGT1A3 was the only one showing no difference in induction by rifampin and nelfinavir. Neither rifampin nor nelfinavir induced the expression of RPLP0, which is not a target gene of PXR.

Figure 7B shows that co-treatment with increasing concentrations of nelfinavir antagonized the induction of ABCB1 and CYP3A4 by rifampin, while the respective effect was not statistically significant for CYP2B6, most likely due to the high variability of CYP2B6 induction by rifampin in this experimental set of hepatocytes. Interestingly, treating the cells with 30 μ M nelfinavir only did not result in stronger induction of the genes, as compared to 10 μ M. In the case of CYP3A4, induction even appeared to be suppressed.

Discussion

We have characterized here in detail the interaction of the HIV protease inhibitor nelfinavir and its major metabolite M8 with PXR. Both compounds act as partial agonists and competitive antagonists of human PXR by binding into the LBP of the receptor. The partial agonist/antagonist properties mainly result from impaired co-activator recruitment.

Nelfinavir and its major metabolite M8, which accounts for 80 to 90% of primary metabolites detected in human plasma (Zhang et al., 2001), exert the same functional effects on PXR, thus it is not expected that hepatic metabolism of the drug may limit modulation of the receptor. M8 selectively activated PXR, while nelfinavir also induced the activity of FXR and, as already reported (Lynch et al., 2015), inhibited CAR. In the antagonist mode, slight inhibition of the ligand-dependent activation of several other nuclear receptors by 10 μ M M8 was observed (see Fig. 1C and Suppl. Fig. S2), which however cannot be excluded to result from partial cytotoxicity. Even if the inhibition by 10 μ M M8 would reflect true antagonism of the activity of these nuclear receptors, the biological relevance of such small effects is still questionable.

Direct binding of nelfinavir and M8 to PXR was suggested by docking into the LBP of the receptor's X-ray crystal structures. Neither the AF-2 groove nor any of the identified potential alternative binding sites seem to be suited to favorably bind any of both compounds. Binding of nelfinavir to the LBP appeared to be more favorable compared to M8, as nelfinavir showed a clear preference for a specific binding mode. This may explain the lower EC₅₀ and IC₅₀ values determined for the parent drug. As nelfinavir is a more hydrophobic compound (logP: 4.7) compared to M8 (logP: 3.7), nelfinavir binding to the largely hydrophobic PXR-LBP might be more favorable.

The limited proteolytic digestion and TR-FRET-based competitive ligand binding assays, performed here, showed for the first time experimental evidence that nelfinavir and its metabolite M8 bind to the LBD of PXR. Using a radioligand binding competition assay, Dussault et al. failed to demonstrate binding of nelfinavir to PXR (Dussault et al., 2001). Nevertheless, mean inhibition by 20-25% is visible in the respective data, which the authors regarded as irrelevant. It may be argued that

protection from digestion by trypsin is simply reflecting direct protease inhibition by nelfinavir and its metabolite. However, omitting the ligand pre-incubation step in the limited proteolytic digestion experiment, and only adding the compounds together with trypsin, resulted in a strong decrease in protection of PXR from digestion by the protease. The residual protection is most likely due to ligand binding during the co-incubation with trypsin, as it was likewise observed with T0901317 (data not shown). Accordingly, it has been reported that nelfinavir does not inhibit trypsin activity (Singh et al., 2009; Wignot et al., 2004). The result of the limited proteolytic digestion assay was confirmed by the TR-FRET-based PXR ligand binding competition assay, which further demonstrated nelfinavir and M8 EC₅₀ values for binding to the PXR LBD comparable with respective EC₅₀ of the potent PXR agonist SR12813. Ligand binding of nelfinavir and M8 does not necessarily disqualify an indirect activation mechanism by the inhibition of protein kinases. This mechanism may additionally contribute to activation of PXR by nelfinavir and may further limit nelfinavir-dependent antagonism. Final proof that kinase inhibition contributed to nelfinavir-dependent PXR modulation awaits the analysis of PXR protein phosphorylation following treatment with the drug.

EC₅₀ value in the range of 0.1 μ M for in vitro binding to PXR indicates physiological relevance of the modulation of PXR activity by nelfinavir. The drug shows extremely high intracellular accumulation (Jones et al., 2001; Mateus et al., 2017). Treatment of lymphoblastoid CEM cells with 10 μ M nelfinavir for 18 hours resulted in intracellular concentration of approximately 700 μ M (Jones et al., 2001). As the fraction of unbound intracellular nelfinavir was determined in different cell lines to range from 0.0001 to 0.0004 (Mateus et al., 2017), unbound intracellular concentration can be roughly estimated to range from 0.1 to 0.3 μ M, which can be expected as sufficient for PXR activity modulation. Furthermore, dosing mice with nelfinavir in a way that resulted in similar blood concentrations as the therapeutic dosing of HIV patients, subsequently produced amounts in liver, which corresponded to intracellular amounts in HeLa cells, treated with 5-10 μ M NFV for 6 hours (de Gassart et al., 2016). These data provide indirect evidence that the intracellular concentrations of nelfinavir, which were achieved by treatment of cells with 10 μ M of the compound in the culture medium, thereby exerting PXR-dependent effects, can be expected in vivo in the liver by therapeutic

dosing. Physiological relevance is further supported by induction of endogenous gene expression in primary human hepatocytes by 10 μ M nelfinavir (see Fig. 7A). Nelfinavir may have demonstrated gene-specific induction, as only part of the genes, which have been analyzed, were induced by the drug. These include CYP2B6, CYP2C8, CYP3A4, EPHX1 and UGT1A3, while ABCB1, AKR1B10, FASN and SMPDL3A were not induced. Missing induction of ABCB1 is in contrast to previous reports, which demonstrated induction of the gene (Dixit et al., 2007, Liu et al., 2012). The difference may be explained by donor-dependent gene expression variability of primary human hepatocytes.

Nelfinavir was proven here to act as both a partial agonist and a competitive antagonist of PXR, inhibiting activation by pure agonists, such as rifampin and T0901317, in hepatic cells. These characteristics are mainly due to the impaired recruitment of co-activators, while co-repressor release is not compromised, as compared to a full agonist. In this respect, nelfinavir equals partial agonists of PPAR γ , such as GW0072, FK614 or PA-082 (Oberfield et al., 1999; Fujimura et al., 2005; Burgermeister et al., 2006), which were proven to be selective receptor modulators. In CV-1 cells, nelfinavir neither activated a fusion protein of the GAL4-DBD with the PXR-LBD nor resulted in recruitment of co-activator MED1 (Dussault et al., 2001). This may indicate cell-type specificity and thus selective receptor modulation. Failure of PXR activation in CV-1 cells was not simply due to the use of a GAL4-DBD/PXR-LBD fusion protein. Performing an equivalent experiment in HepG2 cells resulted in the same partial agonism of nelfinavir (Supplemental Fig. S3), as observed with full-length PXR in CYP3A4 reporter assays. Nelfinavir may thus be regarded as a basic structure for the development of specific PXR selective receptor modulators. However, this would require detailed information on the binding mode of nelfinavir in the PXR-LBP, which clearly requires the elucidation of the nelfinavir-bound PXR crystal structure.

We have shown here that nelfinavir competitively antagonized PXR activity, which may be of physiological relevance, as the drug also antagonized PXR-dependent induction of ABCB1 and CYP3A4 in hepatocytes (see Fig. 7B). PXR antagonism by nelfinavir may contribute further to the nelfinavir-dependent re-sensitization of cancer cells to cytotoxic drug treatment (Kim et al., 2019). This applies particularly in the case that the development of chemoresistance had involved PXR

activation. Several anticancer drugs, such as paclitaxel and cisplatin (Masuyama et al., 2005), vincristine and vinblastine (Harmsen et al., 2010), SN-38, the active metabolite of irinotecan (Basseville et al., 2011) and sorafenib (Feng et al., 2018) were shown to bind to and/or activate PXR. Chemoresistance generated by treatment with these drugs may thus have been caused by PXR activation (Planque et al., 2016; Feng et al., 2018). Consequently, PXR antagonists may re-sensitize chemoresistant cancer cells. This concept was recently validated by the re-sensitization of cisplatin-resistant HepG2 cells by treatment with the PXR antagonist leflunomide (Yasuda et al., 2019). However, the PXR-dependent effects of nelfinavir in cancer cells and especially in chemoresistant cancer cells require further study.

Modulation of PXR by nelfinavir may not necessarily result in anti-cancer activity. In models of breast, prostate or colorectal cancer, PXR induces tumor progression and chemo-resistance (Pondugula et al., 2016). If PXR has not yet been activated in such a context, treatment with nelfinavir may activate the receptor and counteract nelfinavir-dependent anti-cancer pathways. However, if PXR has already been activated, nelfinavir may antagonize this activation and result in tumor suppression or counteract PXR-induced chemo-resistance. Here, PXR antagonism might synergize with other anti-cancer pathways, which are triggered by nelfinavir. It is the other way round in cancers, where PXR acts as a tumor suppressor. Consequently, the here described partial agonism and competitive antagonism of nelfinavir in the modulation of PXR activity have to be considered, if nelfinavir is planned to be used as an anti-cancer drug.

In conclusion, we have elucidated the molecular mechanism of PXR modulation by nelfinavir and its major metabolite M8. Both compounds bind directly to the receptor and act as partial agonists, but also competitively antagonize ligand-mediated PXR activation. Given the current efforts to repurpose nelfinavir as an anticancer drug and considering that PXR plays a role in cancer cell survival pathways and is thought to be involved in the development of chemoresistance, it is important to know how the drug influences PXR activity. The data presented here may thus help to better understand the manifold effects of nelfinavir on cancer cells.

Acknowledgments.

We greatly appreciate the expert technical assistance of K. Abuazi-Rincones (Stuttgart). M. Demmel and colleagues (Biobank, Munich) kindly prepared primary human hepatocytes. This work was supported by the Human Tissue and Cell Research (HTCR) Foundation, a non-profit foundation regulated by German civil law, which facilitates research with human tissue through the provision of an ethical and legal framework for sample collection. B. Spiegelman, T. Tanaka and H. Wang kindly provided plasmids.

Authorship contributions

Participated in research design: Burk, Windshügel

Conducted experiments: Burk, Kronenberger, Keminer, Windshügel

Contributed new reagents or analytical tools: Lee, Schiergens

Performed data analysis: Burk, Kronenberger, Keminer, Windshügel

Wrote or contributed to the writing of the manuscript: Burk, Schwab, Windshügel

References

- Arnold KA, Eichelbaum M, and Burk O (2004) Alternative splicing affects the function and tissue-specific expression of the human constitutive androstane receptor. *Nucl Recept* **2**: 1.
- Basseville A, Preisser L, de Carné Trécesson S, Boisdron-Celle M, Gamelin E, Coqueret O, Morel A (2011) Irinotecan induces steroid and xenobiotic receptor (SXR) signaling to detoxification pathway in colon cancer cells. *Mol Cancer* **10**: 80.
- Berman HM, Westbrook J, Feng Z, Gilliland G, Bhat TN, Weissig H, Shindyalov IN, and Bourne PE. (2000) The Protein Data Bank. *Nucleic Acids Res* **28**: 235-242.
- Bhattarai D, Singh S, Jang Y, Hyeon Han S, Lee K, and Choi Y (2016) An Insight into Drug Repositioning for the Development of Novel Anti-Cancer Drugs. *Curr Top Med Chem* **16**: 2156-2168.
- Bitter A, Rümmele P, Klein K, Kandel BA, Rieger JK, Nüssler AK, Zanger UM, Trauner M, Schwab M, and Burk O (2015) Pregnane X receptor activation and silencing promote steatosis of human hepatic cells by distinct lipogenic mechanisms. *Arch Toxicol* **89**: 2089-2103.
- Burgermeister E, Schnoebelen A, Flament A, Benz J, Stihle M, Gsell B, Rufer A, Ruf A, Kuhn B, Märki HP, Mizrahi J, Sebokova E, Niesor E, and Meyer M (2006) A novel partial agonist of peroxisome proliferator-activated receptor-gamma (PPARgamma) recruits PPARgamma-coactivator-1alpha, prevents triglyceride accumulation, and potentiates insulin signaling in vitro. *Mol Endocrinol* **20**: 809-830.
- Burk O, Arnold KA, Nussler AK, Schaeffeler E, Efimova E, Avery BA, Avery MA, Fromm MF, and Eichelbaum M (2005) Antimalarial artemisinin drugs induce cytochrome P450 and MDR1 expression by activation of xenosensors pregnane X receptor and constitutive androstane receptor. *Mol Pharmacol* **67**: 1954-1965.

Burk O, Kuzikov M, Kronenberger T, Jeske J, Keminer O, Thasler WE, Schwab M, Wrenger C, and Windshügel B (2018) Identification of approved drugs as potent inhibitors of pregnane X receptor activation with differential receptor interaction profiles. *Arch Toxicol* **92**: 1435-1451.

Burk O, Tegude H, Koch I, Hustert E, Wolbold R, Glaeser H, Klein K, Fromm MF, Nuessler AK, Neuhaus P, Zanger UM, Eichelbaum M, and Wojnowski L (2002) Molecular mechanisms of polymorphic CYP3A7 expression in adult human liver and intestine. *J Biol Chem* **277**: 24280-24288.

De Gassart A, Bujisic B, Zaffalon L, Decosterd LA, Di Micco A, Frera G, Tallant R, Martinon F (2016) An inhibitor of HIV-1 protease modulates constitutive eIF2 α dephosphorylation to trigger a specific integrated stress response. *Proc Natl Acad Sci USA* **113**: E117-126.

Dixit V, Hariparsad N, Li F, Desai P, Thummel KE, and Unadkat JD (2007) Cytochrome P450 enzymes and transporters induced by anti-human immunodeficiency virus protease inhibitors in human hepatocytes: implications for predicting clinical drug interactions. *Drug Metab Dispos* **35**: 1853-1859.

Dong H, Lin W, Wu J, Chen T (2010) Flavonoids activate pregnane x receptor-mediated CYP3A4 gene expression by inhibiting cyclin-dependent kinases in HepG2 liver carcinoma cells. *BMC Biochem* **11**: 23.

Dussault I, Lin M, Hollister K, Wang EH, Synold TW, and Forman BM (2001) Peptide mimetic HIV protease inhibitors are ligands for the orphan receptor SXR. *J Biol Chem* **276**: 33309-33312.

Feng F, Jiang Q, Cao S, Cao Y, Li R, Shen L, Zhu H, Wang T, Sun L, Liang E, Sun H, Chai Y, Li X, Liu G, Yang R, Yang Z, Yang Y, Xin S, Li BA (2018) Pregnane X receptor mediates sorafenib resistance in advanced hepatocellular carcinoma. *Biochim Biophys Acta Gen Subj* **1862**: 1017-1030.

Forman BM, Tontonoz P, Chen J, Brun RP, Spiegelman BM, and Evans RM (1995) 15-Deoxy- δ 12, 14-prostaglandin J2 is a ligand for the adipocyte determination factor PPAR gamma. *Cell* **83**: 803-812.

Fujimura T, Sakuma H, Konishi S, Oe T, Hosogai N, Kimura C, Aramori I, and Mutoh S (2005)

FK614, a novel peroxisome proliferator-activated receptor gamma modulator, induces differential transactivation through a unique ligand-specific interaction with transcriptional coactivators. *J Pharmacol Sci* **99**: 342-352.

Geick A, Eichelbaum M, and Burk O (2001) Nuclear receptor response elements mediate induction of intestinal MDR1 by rifampin. *J Biol Chem* **276**: 14581-14587.

Guan M, Fousek K, Jiang C, Guo S, Synold T, Xi B, Shih CC, and Chow WA (2011) Nelfinavir induces liposarcoma apoptosis through inhibition of regulated intramembrane proteolysis of SREBP-1 and ATF6. *Clin Cancer Res* **17**: 1796-1806.

Gupta A, Mugundu GM, Desai PB, Thummel KE, and Unadkat JD (2008) Intestinal human colon adenocarcinoma cell line LS180 is an excellent model to study pregnane X receptor, but not constitutive androstane receptor, mediated CYP3A4 and multidrug resistance transporter 1 induction: studies with anti-human immunodeficiency virus protease inhibitors. *Drug Metab Dispos* **36**: 1172-1180.

Gupta AK, Li B, Cerniglia GJ, Ahmed MS, Hahn SM, and Maity A (2007) The HIV protease inhibitor nelfinavir downregulates Akt phosphorylation by inhibiting proteasomal activity and inducing the unfolded protein response. *Neoplasia* **9**: 271-278.

Harmsen S, Meijerman I, Febus CL, Maas-Bakker RF, Beijnen JH, Schellens JH (2010) PXR-mediated induction of P-glycoprotein by anticancer drugs in a human colon adenocarcinoma-derived cell line. *Cancer Chemother Pharmacol* **66**: 765-771.

Hoffart E, Ghebreghiorgis L, Nussler AK, Thasler WE, Weiss TS, Schwab M, and Burk O (2012) Effects of atorvastatin metabolites on induction of drug-metabolizing enzymes and membrane transporters through human pregnane X receptor. *Br J Pharmacol* **165**: 1595-1608.

Huang L, Wring SA, Woolley JL, Brouwer KR, Serabjit-Singh C, and Polli JW (2001) Induction of P-glycoprotein and cytochrome P450 3A by HIV protease inhibitors. *Drug Metab Dispos* **29**: 754-760.

- Hustert E, Zibat A, Presecan-Siedel E, Eiselt R, Mueller R, Fuss C, Brehm I, Brinkmann U, Eichelbaum M, Wojnowski L, and Burk O (2001) Natural protein variants of pregnane X receptor with altered transactivation activity toward CYP3A4. *Drug Metab Dispos* **29**: 1454-1459.
- Jeske J, Windshügel B, Thasler WE, Schwab M, and Burk O (2017) Human pregnane X receptor is activated by dibenzazepine carbamate-based inhibitors of constitutive androstane receptor. *Arch Toxicol* **91**: 2375-2390.
- Jiang W, Mikochik PJ, Ra JH, Lei H, Flaherty KT, Winkler JD, and Spitz FR (2007) HIV protease inhibitor nelfinavir inhibits growth of human melanoma cells by induction of cell cycle arrest. *Cancer Res* **67**: 1221-1227.
- Jones K, Hoggard PG, Sales SD, Khoo S, Davey R, Back DJ (2001) Differences in the intracellular accumulation of HIV protease inhibitors in vitro and the effect of active transport. *AIDS* **15**: 675-681.
- Kim JY, Park YJ, Lee BM, and Yoon S (2019) Co-treatment With HIV Protease Inhibitor Nelfinavir Greatly Increases Late-phase Apoptosis of Drug-resistant KBV20C Cancer Cells Independently of P-Glycoprotein Inhibition. *Anticancer Res* **39**: 3757-3765.
- Koltai T (2015) Nelfinavir and other protease inhibitors in cancer: mechanisms involved in anticancer activity. Version 2. *F1000Res* **4**: 9.
- Laskowski RA, MacArthur MW, Moss DS, and Thornton JM (1993) PROCHECK-a program to check the stereochemical quality of protein structures. *J Appl Cryst* **26**: 283-291.
- Lee SM, Schelcher C, Demmel M, Hauner M, and Thasler WE (2013) Isolation of human hepatocytes by a two-step collagenase perfusion procedure. *J Vis Exp* (**79**): e50615.
- Lin W, Wang YM, Chai SC, Lv L, Zheng J, Wu J, Zhang Q, Wang YD, Griffin PR, Chen T (2017) SPA70 is a potent antagonist of human pregnane X receptor. *Nat Commun* **8**: 741.

Lin W, Wu J, Dong H, Bouck D, Zeng FY, and Chen T (2008) Cyclin-dependent kinase 2 negatively regulates human pregnane X receptor-mediated CYP3A4 gene expression in HepG2 liver carcinoma cells. *J Biol Chem* **283**: 30650-30657.

Liu L, Mugundu GM, Kirby BJ, Samineni D, Desai PB, and Unadkat JD (2012) Quantification of human hepatocyte cytochrome P450 enzymes and transporters induced by HIV protease inhibitors using newly validated LC-MS/MS cocktail assays and RT-PCR. *Biopharm Drug Dispos* **33**: 207-217.

Lynch C, Zhao J, Huang R, Xiao J, Li L, Heyward S, Xia M, and Wang H (2015) Quantitative high-throughput identification of drugs as modulators of human constitutive androstane receptor. *Sci Rep* **5**: 10405.

Mackowiak B, and Wang H (2016) Mechanisms of xenobiotic receptor activation: Direct vs. indirect. *Biochim Biophys Acta* **1859**: 1130-1140.

Masuyama H, Suwaki N, Tateishi Y, Nakatsukasa H, Segawa T, Hiramatsu Y (2005) The pregnane X receptor regulates gene expression in a ligand- and promoter-selective fashion. *Mol Endocrinol* **19**: 1170-80.

Mateus A, Treyer A, Wegler C, Karlgren M, Matsson P, Artursson P (2017) Intracellular drug bioavailability: a new predictor of system dependent drug disposition. *Sci Rep* **7**: 43047.

Oberfield JL, Collins JL, Holmes CP, Goreham DM, Cooper JP, Cobb JE, Lenhard JM, Hull-Ryde EA, Mohr CP, Blanchard SG, Parks DJ, Moore LB, Lehmann JM, Plunket K, Miller AB, Milburn MV, Kliewer SA, and Willson TM (1999) A peroxisome proliferator-activated receptor gamma ligand inhibits adipocyte differentiation. *Proc Natl Acad Sci U S A* **96**: 6102-6106.

Pascussi JM, Gerbal-Chaloin S, Drocourt L, Maurel P, and Vilarem MJ (2003) The expression of CYP2B6, CYP2C9 and CYP3A4 genes: a tangle of networks of nuclear and steroid receptors. *Biochim Biophys Acta* **1619**: 243-253.

Piedade R, Traub S, Bitter A, Nüssler AK, Gil JP, Schwab M, and Burk O (2015)

Carboxymefloquine, the major metabolite of the antimalarial drug mefloquine, induces drug-metabolizing enzyme and transporter expression by activation of pregnane X receptor. *Antimicrob Agents Chemother* **59**: 96-104.

Planque C, Rajabi F, Grillet F, Finetti P, Bertucci F, Gironella M, Lozano JJ, Beucher B, Giraud J, Garambois V, Vincent C, Brown D, Caillo L, Kantar J, Pelegrin A, Prudhomme M, Ripoche J, Bourgaux JF, Ginestier C, Castells A, Hollande F, Pannequin J, and Pascussi JM (2016) Pregnane X-receptor promotes stem cell-mediated colon cancer relapse. *Oncotarget* **7**: 56558-56573.

Pondugula SR, Pavak P, and Mani S (2016) Pregnane X Receptor and Cancer: Context-Specificity is Key. *Nucl Receptor Res* **3**: 101198.

Prakash C, Zuniga B, Song CS, Jiang S, Cropper J, Park S, and Chatterjee B (2015) Nuclear Receptors in Drug Metabolism, Drug Response and Drug Interactions. *Nucl Receptor Res* **2**: 101178.

Riedmaier S, Klein K, Hofmann U, Keskitalo JE, Neuvonen PJ, Schwab M, Niemi M, and Zanger UM (2010) UDP-glucuronosyltransferase (UGT) polymorphisms affect atorvastatin lactonization in vitro and in vivo. *Clin Pharmacol Ther* **87**: 65-73.

Shim JS, and Liu JO (2014) Recent advances in drug repositioning for the discovery of new anticancer drugs. *Int J Biol Sci* **10**: 654-663.

Shim JS, Rao R, Beebe K, Neckers L, Han I, Nahta R, and Liu JO (2012) Selective inhibition of HER2-positive breast cancer cells by the HIV protease inhibitor nelfinavir. *J Natl Cancer Inst* **104**: 1576-1590.

Singh VP, Bren GD, Algeciras-Schimmich A, Schnepple D, Navina S, Rizza SA, Dawra RK, Saluja AK, Chari ST, Vege SS, and Badley AD (2009) Nelfinavir/ritonavir reduces acinar injury but not inflammation during mouse caerulein pancreatitis. *Am J Physiol Gastrointest Liver Physiol* **296**: G1040-G1046.

Sippl MJ (1993) Recognition of errors in three-dimensional structures of proteins. *Proteins* **17**: 355-362.

Svärd J, Spiers JP, Mulcahy F, and Hennessy M (2010) Nuclear receptor-mediated induction of CYP450 by antiretrovirals: functional consequences of NR1I2 (PXR) polymorphisms and differential prevalence in whites and sub-Saharan Africans. *J Acquir Immune Defic Syndr* **55**: 536-549.

Tachibana K, Kobayashi Y, Tanaka T, Tagami M, Sugiyama A, Katayama T, Ueda C, Yamasaki D, Ishimoto K, Sumitomo M, Uchiyama Y, Kohro T, Sakai J, Hamakubo T, Kodama T, and Doi T (2005) Gene expression profiling of potential peroxisome proliferator-activated receptor (PPAR) target genes in human hepatoblastoma cell lines inducibly expressing different PPAR isoforms. *Nucl Recept* **3**: 3.

Thasler WE, Weiss TS, Schillhorn K, Stoll PT, Irrgang B, and Jauch KW (2003) Charitable state-controlled foundation Human Tissue and Cell Research: ethic and legal aspects in the supply of surgically removed human tissue for research in the academic and commercial sector in Germany. *Cell Tissue Bank* **4**: 49-56.

Wang H, Faucette S, Sueyoshi T, Moore R, Ferguson S, Negishi M, and LeCluyse EL (2003) A novel distal enhancer module regulated by pregnane X receptor/constitutive androstane receptor is essential for the maximal induction of CYP2B6 gene expression. *J Biol Chem* **278**: 14146-14152.

Wang H, Li H, Moore LB, Johnson MD, Maglich JM, Goodwin B, Ittoop OR, Wisely B, Creech K, Parks DJ, Collins JL, Willson TM, Kalpana GV, Venkatesh M, Xie W, Cho SY, Roboz J, Redinbo M, Moore JT, and Mani S (2008) The phytoestrogen coumestrol is a naturally occurring antagonist of the human pregnane X receptor. *Mol Endocrinol* **22**: 838-857.

Wignot TM, Stewart RP, Schray KJ, Das S, and Sipos T (2004) In vitro studies of the effects of HAART drugs and excipients on activity of digestive enzymes. *Pharm Res* **21**: 420-427.

Xie L, Evangelidis T, Xie L, and Bourne PE (2011) Drug discovery using chemical systems biology: weak inhibition of multiple kinases may contribute to the anti-cancer effect of nelfinavir. *PLoS Comput Biol* **7**: e1002037.

Xing Y, Yan J, and Niu Y (2020) PXR: a center of transcriptional regulation in cancer. *Acta Pharm Sin B* **10**: 197-206.

Yasuda M, Kishimoto S, Amano M, Fukushima S (2019) The Involvement of pregnane X receptor-regulated pathways in the antitumor activity of cisplatin. *Anticancer Res* **39**: 3601-3608.

Zhang KE, Wu E, Patick AK, Kerr B, Zorbas M, Lankford A, Kobayashi T, Maeda Y, Shetty B, and Webber S (2001) Circulating metabolites of the human immunodeficiency virus protease inhibitor nelfinavir in humans: structural identification, levels in plasma, and antiviral activities. *Antimicrob Agents Chemother* **45**: 1086-1093.

Footnotes

This work was supported by the Robert Bosch Foundation, Stuttgart, Germany (M.S., O.B.) and the Hamburg Ministry of Science, Research and Equality of the Free and Hanseatic City of Hamburg (B.W.). T.K. was supported by Fundação de Amparo à Pesquisa do Estado de São Paulo (FAPESP, 2014/03644-9 and 2014/27313-1).

Some information presented herein is in the Ph.D. thesis of T.K.: Kronenberger T (2017) Targeting alternative ligand-binding sites in nuclear receptors using computational and experimental screening. Doctoral thesis, University of São Paulo, São Paulo, Brazil (published online at <https://www.teses.usp.br/teses/disponiveis/42/42135/tde-17112017-102040/en.php>).

¹ present address: Department of Internal Medicine VIII, University Hospital Tübingen, Tübingen, Germany and School of Pharmacy, University of Eastern Finland, Kuopio, Finland.

Figure Legends

Fig.1. Effects of nelfinavir and M8 on nuclear receptor activities. (A) Chemical structures of nelfinavir and its active metabolite M8, generated by CYP2C19. (B,C) HepG2 cells were co-transfected with expression plasmids encoding the indicated nuclear receptors and corresponding reporter gene plasmids, as specified in Materials and Methods section. Chemical treatments lasted for 24h. (B) Transfected cells were treated with 0.1% DMSO, or 10 μ M nelfinavir (NFV) or M8. Data are shown as scatter plots with mean (columns) fold induction \pm S.D. ($n=5$) of normalized luciferase activities of the respective reporter genes by chemical treatment, as compared to the corresponding treatments with vehicle DMSO only, which were each designated as 1. Differences to this value were analyzed by one sample t test and P -values were corrected for multiple testing by the method of Bonferroni. (C) Transfected cells were treated with 0.1% DMSO or corresponding prototypical nuclear receptor agonists, as specified in Materials and Methods section, without or with 10 μ M nelfinavir (NFV) or M8. Data are presented as shown above, with means \pm S.D. ($n=5$). Differences to treatments with respective agonists only, were analyzed by repeated measures one-way ANOVA with Dunnett's multiple comparisons test. * $P<0.05$; ** $P<0.01$; *** $P<0.001$

Fig. 2. In silico analysis of PXR binding of nelfinavir and M8. (A) Location of alternative binding sites, indicated by colored alpha spheres (1M13, green: 1NRL:A, cyan; 1NRL:B, magenta; 2O9I:A, red) on the PXR LBD (orange ribbon) The SRC-1 peptide, indicating the location of the AF-2 groove, is shown as grey ribbon. The LBP-bound ligand SR12813 is shown as ball-and-stick representation with carbon atoms in grey. Comparison of the binding modes of (B) M8 and (C) nelfinavir, docked into the PXR-LBP. Different colors indicate the top-ranked conformation of each cluster using a RMSD cut-off of 1.5 Å.

Fig. 3. Analysis of in vitro binding of nelfinavir and M8 to PXR-LBD. (A) Limited proteolytic digestion analysis of PXR-LBD protein, which was incubated with 30, 100 or 250 μ M nelfinavir

(NFV) or M8, 30 μ M T0901317 (T09) or 2.5% DMSO. Upper panel shows the radioluminographic scan of a representative experiment, with 36 kDa undigested input protein (arrow) and protected proteolytic fragments of 32, 26 and 23 kDa (arrow heads). Lower panel shows the respective densitometric quantifications of the sum of the three protected fragments, calculated as percent of input. Data are presented as scatter plots with means (columns) \pm S.D. ($n=5$). Differences to incubation with vehicle DMSO only were analyzed by repeated measures one-way ANOVA with Dunnett's multiple comparisons test. * $P<0.05$; ** $P<0.01$; *** $P<0.001$. (B) Competitive ligand binding to the PXR-LBD using the LanthaScreen® TR-FRET kit. Concentration-dependent response is shown for the indicated compounds between 0.5 nM and 30 μ M as mean of relative binding (%) \pm S.D. from two independent experiments, each done in technical triplicates. Relative binding was calculated as described in Materials and Methods. 2% DMSO was used as negative control and 30 μ M SR12813 as positive control (100% relative binding).

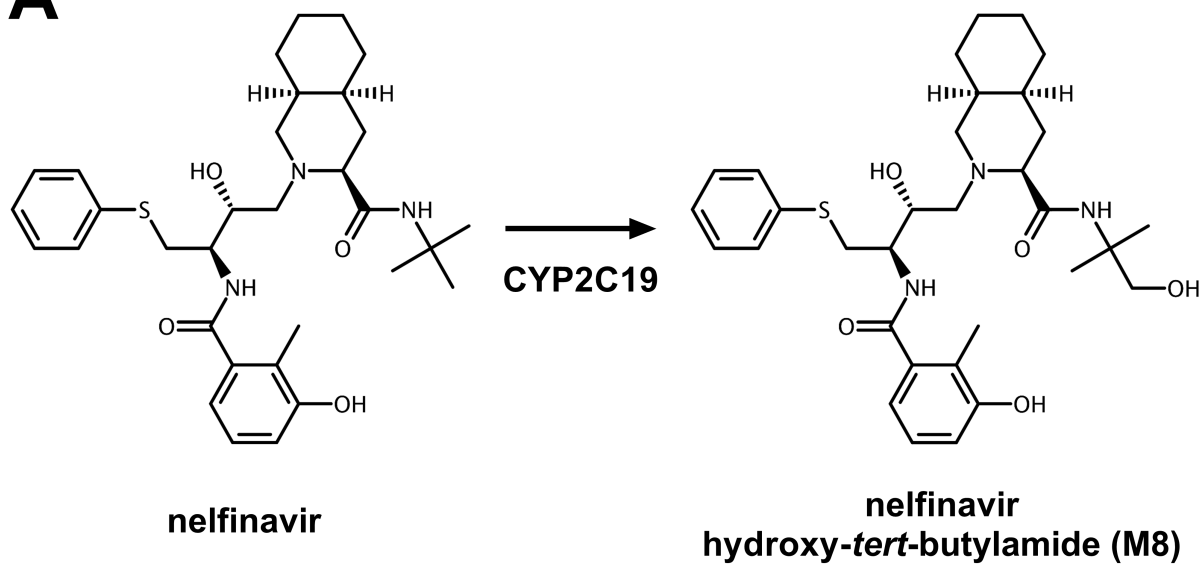
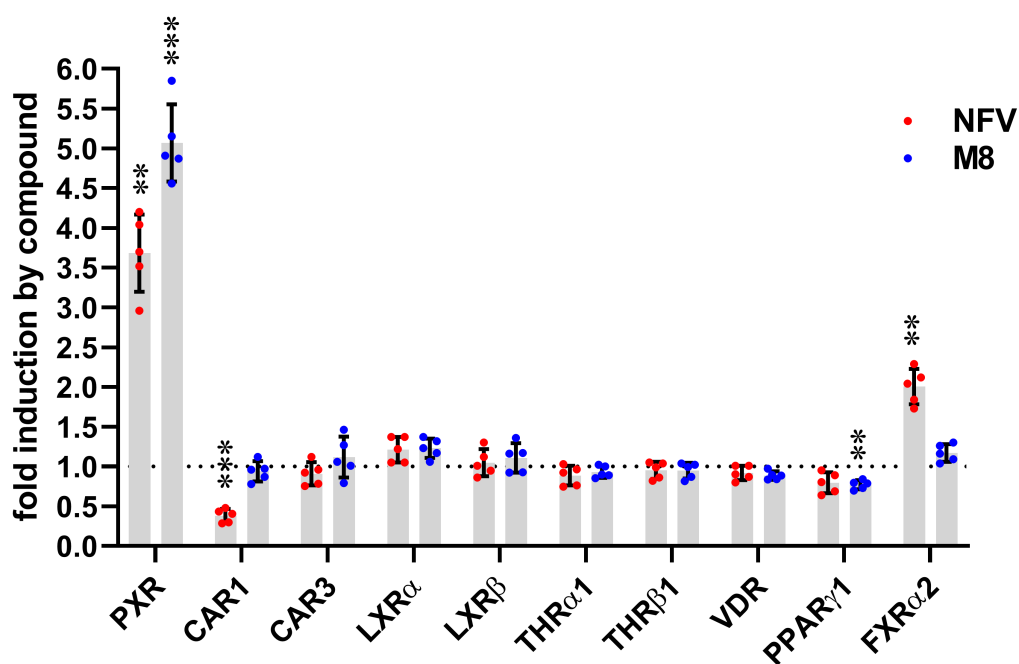
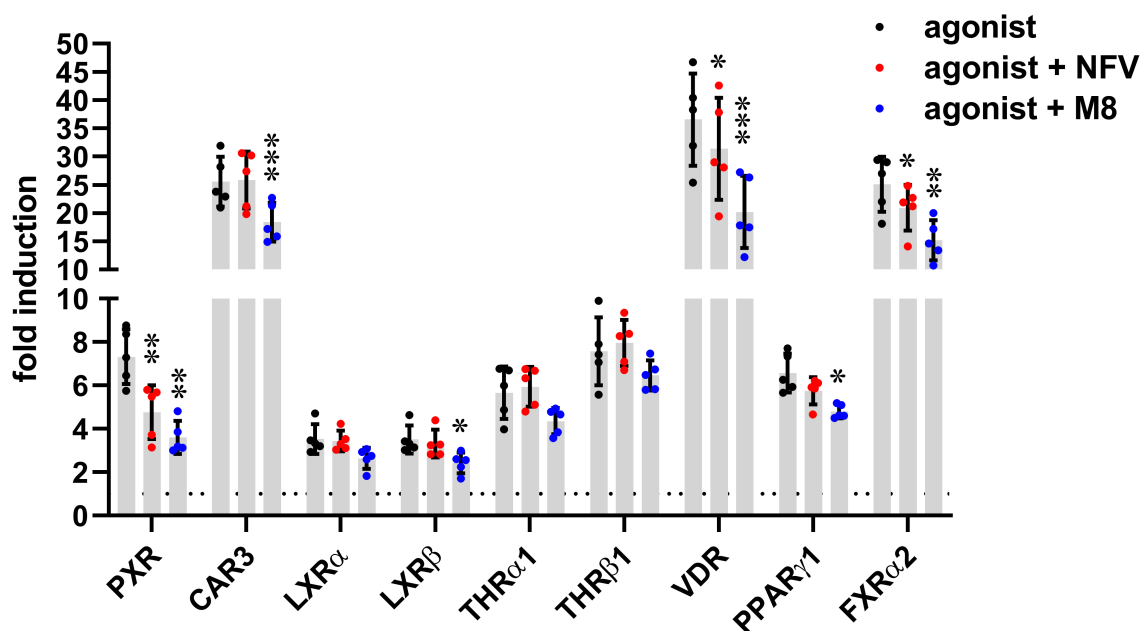
Fig. 4. Concentration-dependent response of PXR activation by nelfinavir and M8 and antagonistic effects on activation by rifampin. H-P cells were transfected with CYP3A4 reporter and (A) treated for 24h with increasing concentrations of rifampin (RIF), nelfinavir (NFV) or M8, (B) treated with increasing concentrations of nelfinavir or M8 in the presence or absence of 3 μ M SPA70, (C,D) co-treated with increasing concentrations of rifampin in the presence of the indicated fixed concentrations of (C) nelfinavir or (D) M8, and (E) co-treated with increasing concentrations of nelfinavir or M8 in the presence of 10 μ M rifampin. Mean fold induction \pm S.D. ($n\geq 5$) by the respective treatment is shown, with respect to the normalized reporter activity of cells treated with vehicle DMSO only, which was designated as 1. Non-linear fit of concentration-dependent response was performed with bottom values fixed to 1 in (A) and (F). (E) Panel shows the means \pm standard error of rifampin \log_{10} EC₅₀ values derived from experiments shown in C and D ($n=5$), which have been calculated as described in Materials and Methods. Differences to rifampin \log_{10} EC₅₀ values in the absence of nelfinavir or M8 were analyzed by one-way ANOVA with Dunnett's multiple comparisons test, according to GraphPad Prism knowledgebase article 144 (GraphPad Software,

accessed 17 August 2020, <https://www.graphpad.com/support/faq/how-can-i-test-for-differences-among-three-or-more-curves-fitted-to-three-or-more-data-sets/>).

Fig. 5. Analysis of the effect of nelfinavir on LBP-filled PXR mutant. HepG2 cells were transfected with empty expression vector pcDNA3 (negCTR), or expression plasmids encoding wild-type PXR or the LBP-filled triple PXR mutant S208W/S247W/C284W and treated for 24h with 0.1% DMSO or 10 μ M nelfinavir (NFV) with or without 10 μ M rifampin (RIF). Normalized luciferase activities of co-transfected CYP3A4 reporter are presented in scatter plots with means (columns) \pm S.D. ($n=5$), relative to the activity of cells transfected with pcDNA3 and treated with DMSO only. Differences to respective treatments with DMSO (asterisks, exclusively for single compound treatments) or with rifampin only (daggers, exclusively for nelfinavir + rifampin co-treatment) were analyzed by repeated measures 2-way ANOVA with Dunnett's or Sidak's multiple comparisons tests, respectively. *, $P<0.05$; ††† $P<0.001$

Fig. 6. Effects of nelfinavir on PXR-LBD assembly and transcriptional co-factor interaction. (A) HepG2 cells were co-transfected with combinations of expression plasmids encoding GAL4-DBD/PXR-LBD(132-188) and VP16-AD/PXR-LBD(189-434) or empty vector pVP16-AD. (B-E) HepG2 cells were co-transfected with expression plasmids encoding VP16-AD/PXR-LBD(108-434) fusion protein or empty vector pVP16-AD and expression plasmids encoding fusion proteins of (B) GAL4-DBD/NCOR2-RID, (C) GAL4-DBD/NCOA1-RID, (D) GAL4-DBD/NCOA2-RID or (E) GAL4-DBD/MED1-RID. Transfected cells were treated with 0.1% DMSO or 10 μ M nelfinavir (NFV), with or without 10 μ M rifampin (RIF) for 24 h. Data are presented as scatter plots with means (columns) \pm S.D. ($n=5$) of normalized luciferase activity of the co-transfected pGL3-G5, relative to the activity of cells transfected with pVP16-AD and treated with DMSO only. Differences to respective treatments with DMSO (asterisks, exclusively for single compound treatments) or with rifampin only (daggers, exclusively for nelfinavir + rifampin co-treatment) were analyzed by repeated measures two-way ANOVA with Dunnett's or Sidak's multiple comparisons tests, respectively. *, † $P<0.05$; **, †† $P<0.01$; ***, ††† $P<0.001$

Fig. 7. Effects of nelfinavir on the expression of endogenous PXR target genes in hepatocytes. (A) Cultures of primary human hepatocytes of six donors were each treated with 0.1% DMSO, 10 μ M rifampin (RIF) or 10 μ M nelfinavir (NFV) for 24h. mRNA expression of the indicated genes was determined by TaqMan RT-qPCR and normalized to the expression of 18S rRNA. Data is presented in scatter plots with medians and interquartile ranges. Expression was calculated as fold induction caused by the respective chemical treatment, as compared to the expression in cells treated with vehicle DMSO only, which was designated as 1. Differences to this value were analyzed by one sample Wilcoxon signed rank tests (asterisks). Differences between rifampin and nelfinavir treatments were analyzed by Wilcoxon matched-pairs signed rank tests for each gene individually (daggers). (B) Cultured primary human hepatocytes of four donors were treated for 24h with 0.1% DMSO or 10 or 30 μ M nelfinavir (NFV), in the absence or presence of 10 μ M rifampin (RIF). mRNA expression of the indicated genes was calculated and is presented as described above. Differences to treatment with rifampin only, were analyzed by Friedman test with Dunn's multiple comparisons test (asterisks, exclusively for co-treatments of rifampin and nelfinavir). *, † $P < 0.05$; ** $P < 0.01$

A**B****C****Figure 1**

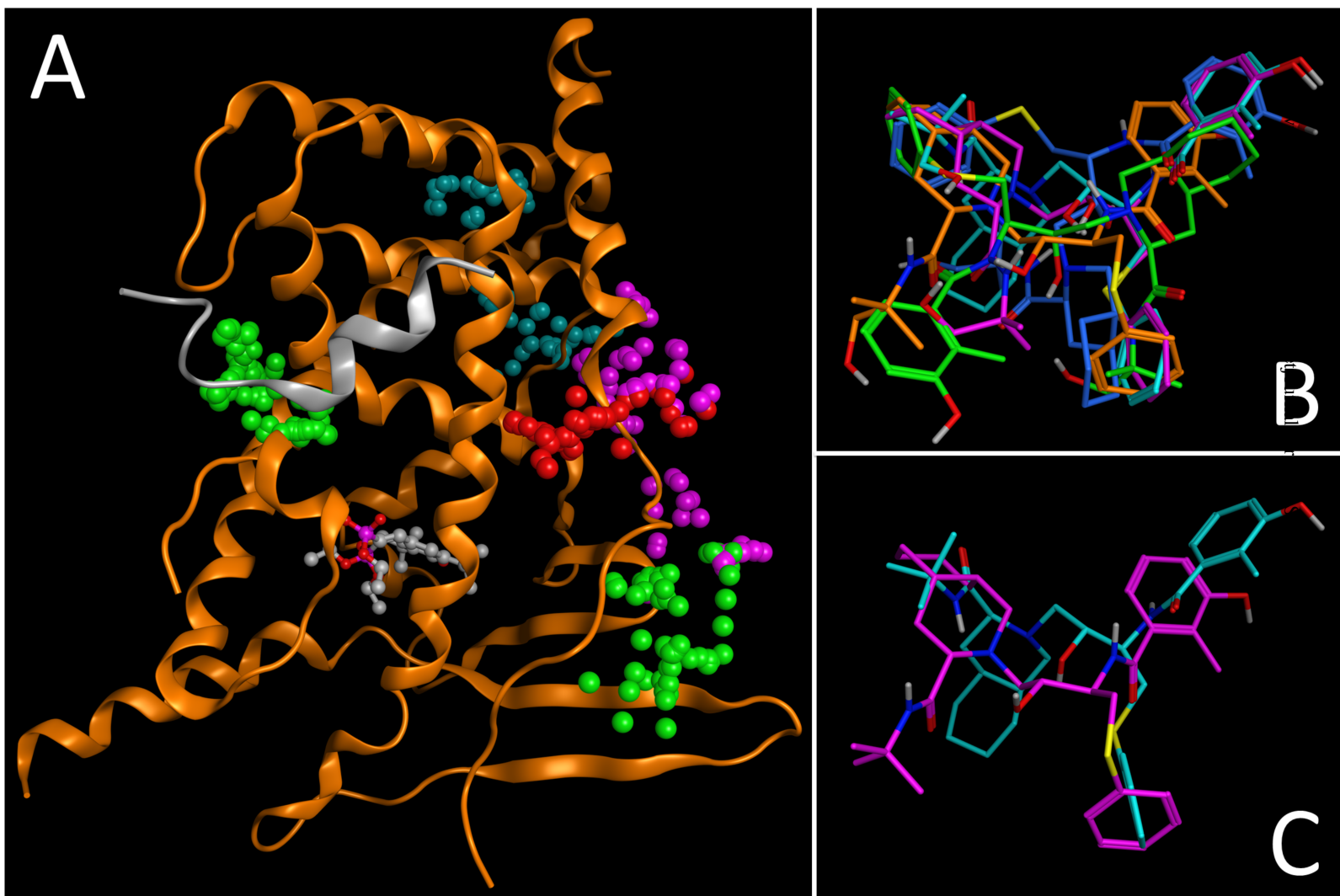
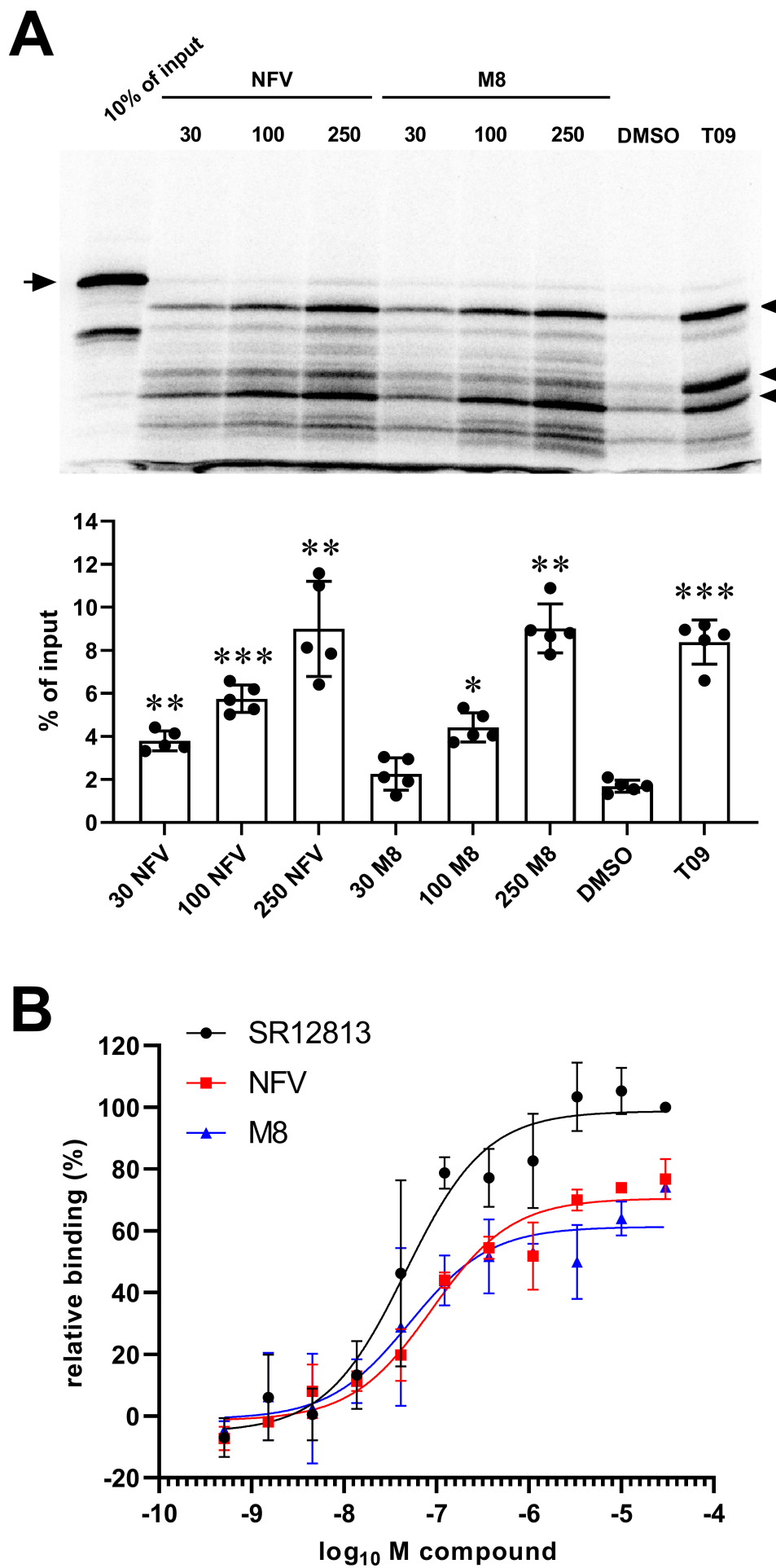


Figure 2

**Figure 3**

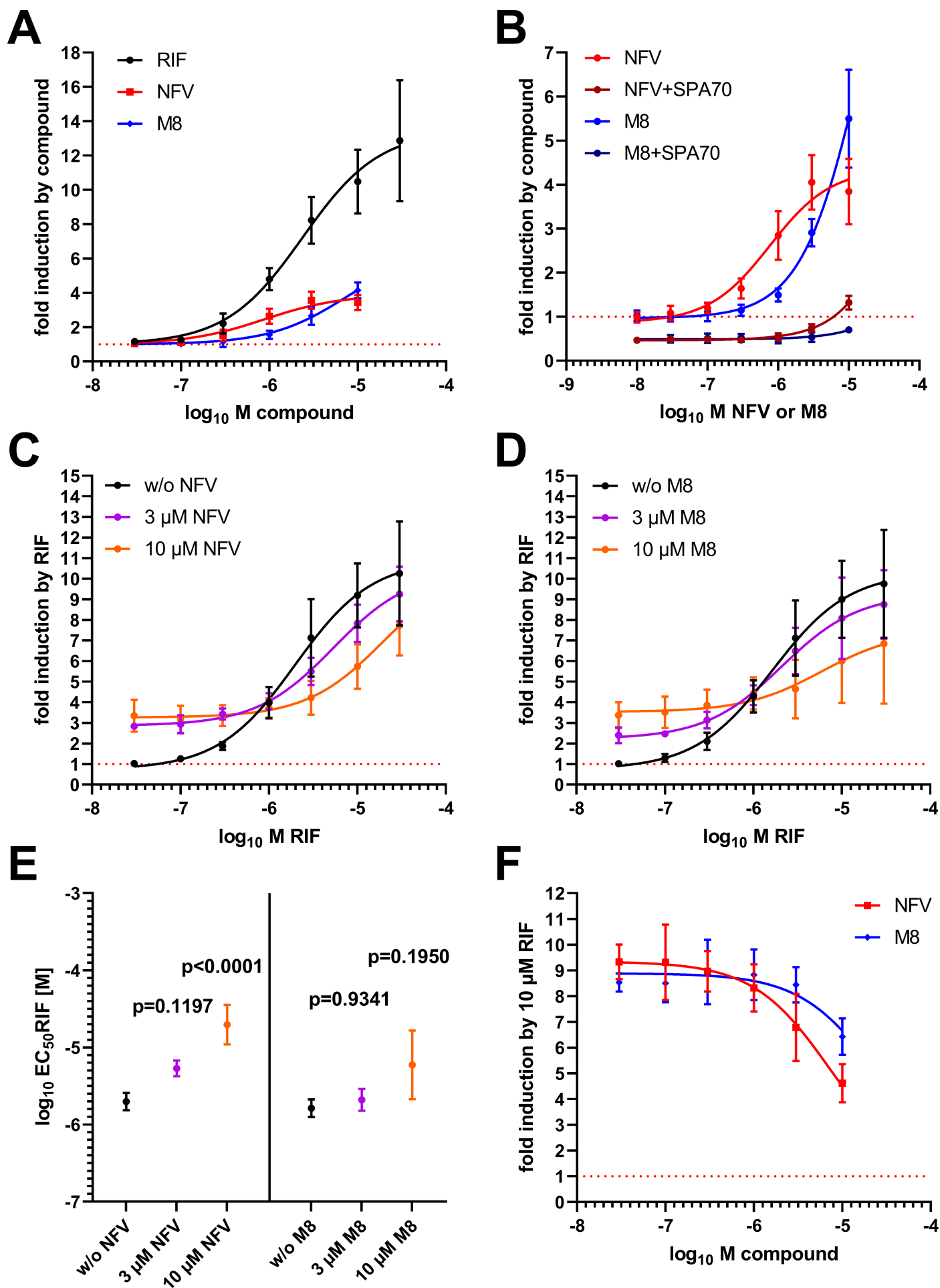


Figure 4

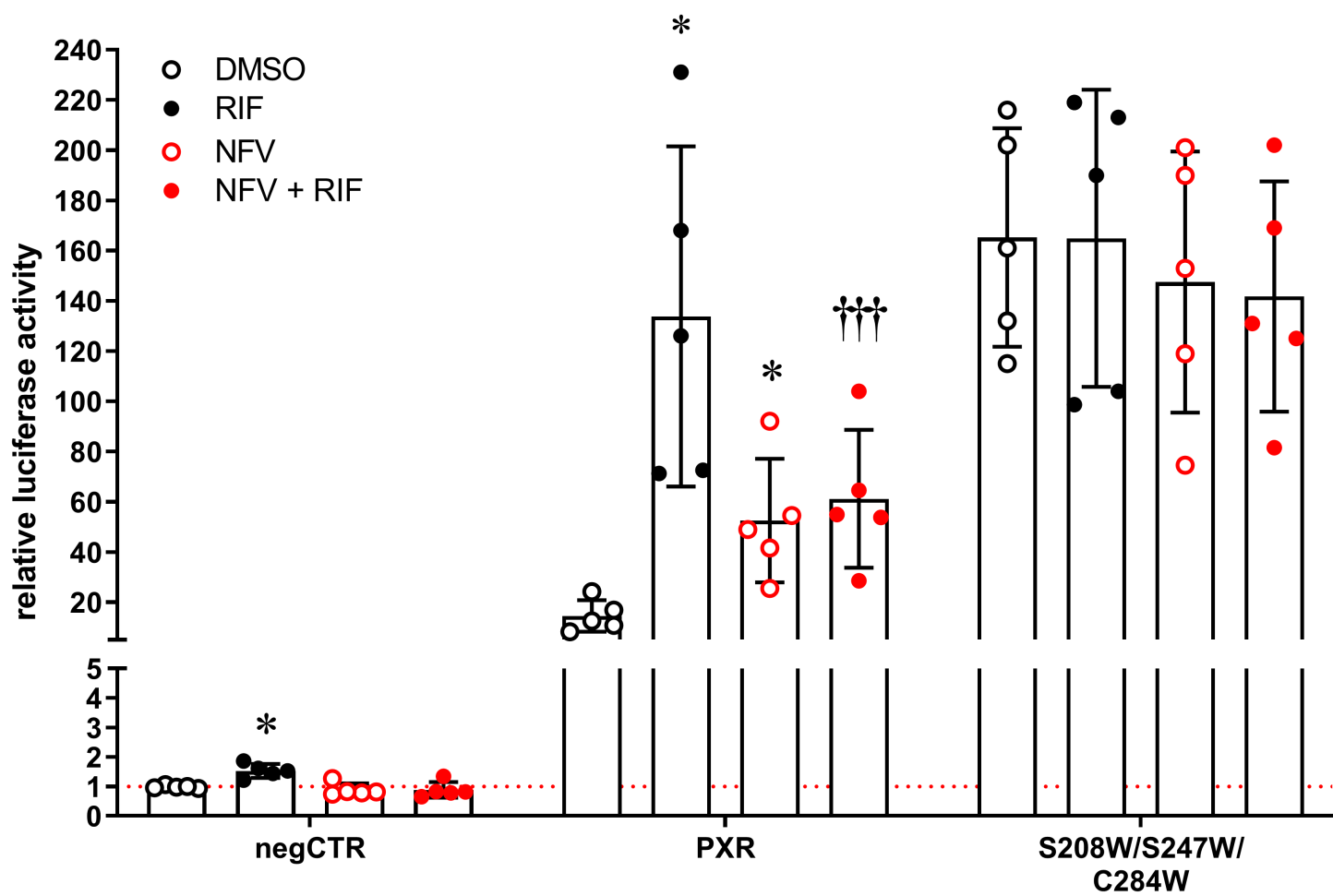


Figure 5

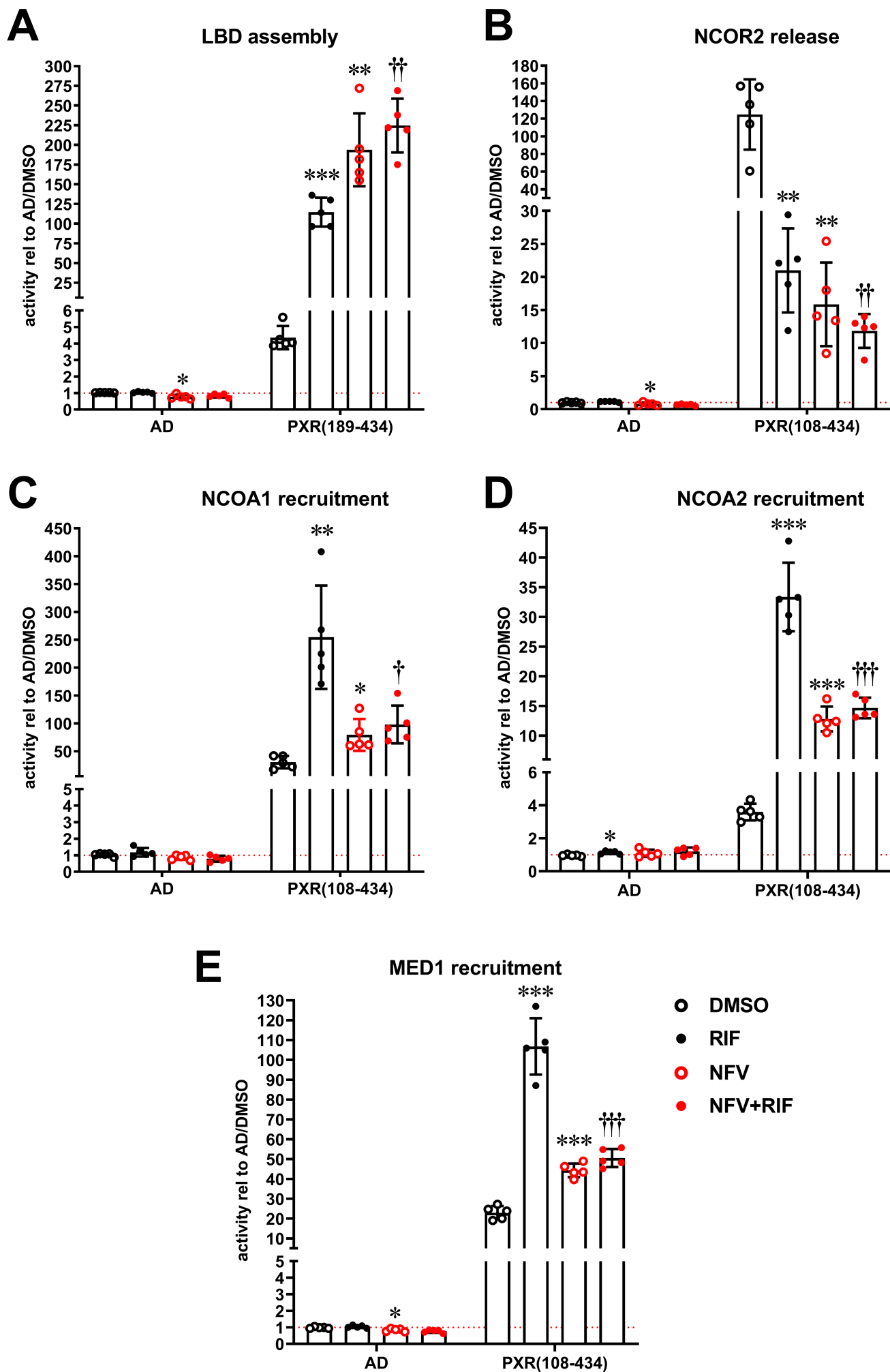


Figure 6

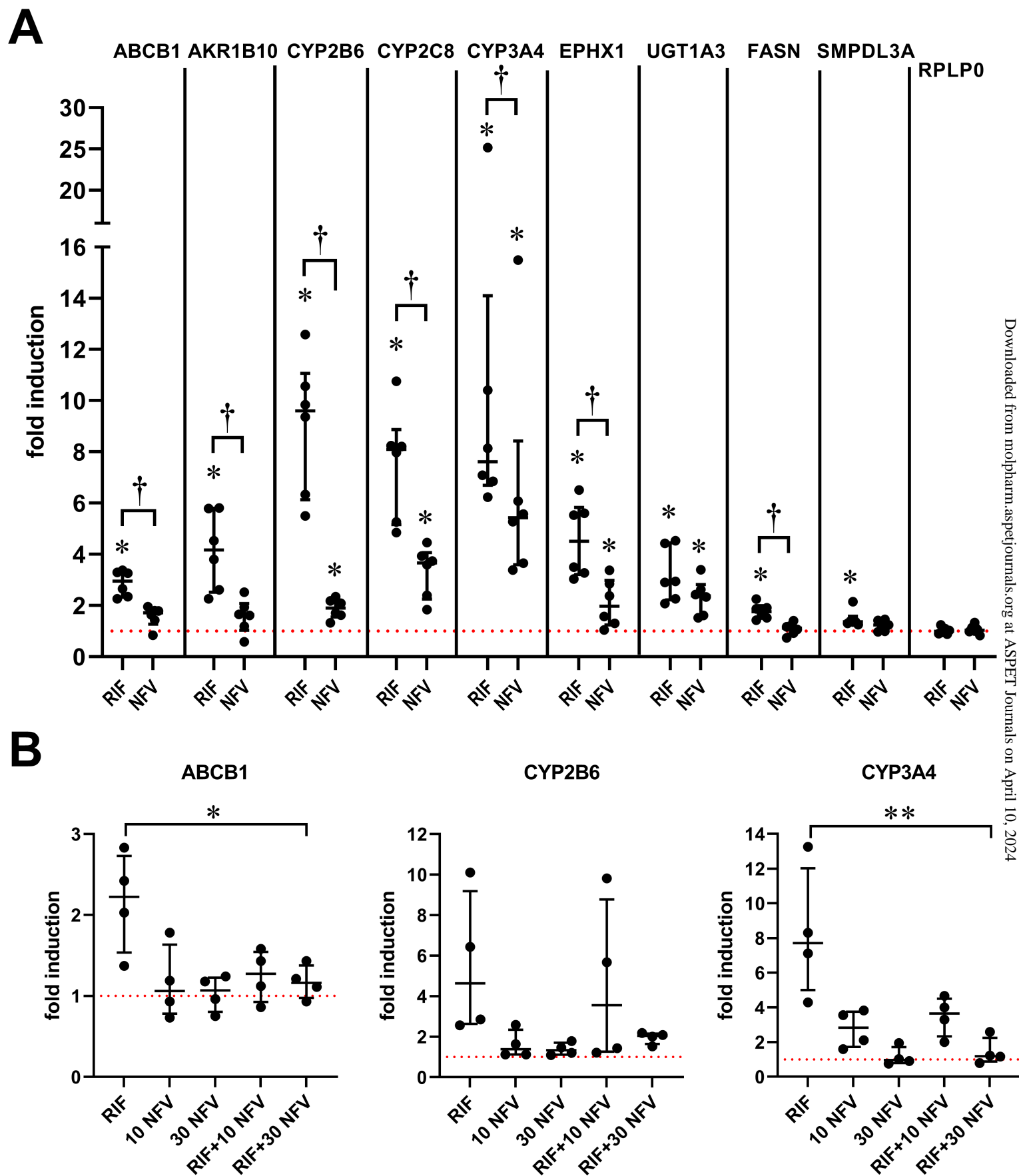


Figure 7

Supplemental Data

Manuscript number: MOLPHARM-AR-2020-000116R1

Nelfinavir and its active metabolite M8 are partial agonists and competitive antagonists of the human pregnane X receptor

Oliver Burk, Thales Kronenberger, Oliver Keminer, Serene M. L. Lee, Tobias S. Schiergens, Matthias Schwab, Björn Windshügel

Supplemental Materials and Methods

Cell viability

HepG2 or H-P cells were seeded into white flat-bottom CELLSTAR® 96-well plates with µClear® bottom (Greiner Bio-One, Frickenhausen, Germany), with 40,000 cells per well in a volume of 100 µl and incubated for 24 hours. Then, cells were treated for further 24 hours with varying doses of nelfinavir or metabolite M8, ranging from 1 to 50 µM, or vehicle only (0.5% DMSO). Each treatment was performed in technical triplicates. Afterwards, cell viability was determined based on ATP content, using the CellTiter-Glo® luminescent cell viability assay (Promega), as specified by the manufacturer. Luminescence was measured with the 2300 EnSpire multimode plate reader (Perkin Elmer, Rodgau, Germany).

Supplemental Table S1 Hepatocyte donor data

ID	ethnicity	sex	age cohort	diagnosis	long-term medication	used in
GH41	European	female	30-39	liver metastasis CRC	n.s.	Fig. 7A
GH42	European	female	50-59	focal nodular hyperplasia	none	Fig. 7A
GH43	European	female	30-39	focal nodular hyperplasia	n.s.	Fig. 7A
GH44	European	male	50-59	liver metastasis CRC	vitamin D	Fig. 7A
GH45	European	female	60-69	liver metastasis CRC	pantoprazole	Fig. 7A
GH46	n.s.	Male	30-39	liver metastasis CRC	pantoprazole	Fig. 7A
GH61	n.s.	female	70-79	liver metastasis breast carcinoma	ramipril, L-thyroxine	Fig. 7B
GH62	European	Male	70-79	liver metastasis CRC	acetylsalicylic acid, bisoprolol, simvastatin, ticagrelor	Fig. 7B
GH63	European	Female	30-39	liver metastasis CRC	tinzaparin	Fig. 7B
GH64	European	Male	60-69	intrahepatic CCC	salbutamol, unspecified hypertensive drug(s), unspecified ACE inhibitor(s)	Fig. 7B

n.s., not specified; CRC, colorectal carcinoma; CCC, cholangiocellular carcinoma

Supplemental Table S2. Overview of binding site characteristics and docking scores.

PDB ID	Pocket	Size	PLB	Docking Scores	
				NFV	M8
1M13	LBP	245	4.6	101.4	104.3
C284 A	AF-2	n.d.	n.d.	77.07	76.2
	Alt-1	60	1.4	82.9	80.3
	Alt-2	56	0.8	68.4	71
1M13	LBP	244	4.6	104.4	106.1
C284 B	AF-2	n.d.	n.d.	75.3	74.8
	Alt-1	60	1.48	78.1	80.7
	Alt 2	64	0.91	66.7	67.8
1NRL	LBP	190	4.4	107.4	110.4
Chain A	AF-2	n.d.	n.d.	76.8	78
	Alt-1	32	1.37	64.7	67.4
	Alt-2	45	1.16	71	66.8
1NRL	LBP	190	3.8	97	100
Chain B	AF-2	n.d.	n.d.	81.1	78.2
	Alt-1	67	1.9	63.7	68.2
	Alt-2	41	1.2	76.3	78.3
2O9I	LBP	186	4	104	103.2
Chain A	AF-2	n.d.	n.d.	75.3	78.5
	Alt-1	52	1.8	73.4	72.1
	Alt-2	46	1	73.9	75.1
2O9I	LBP	186	4	98.4	101
Chain B	AF-2	n.d.	n.d.	84.2	85.4
	Alt-1	52	1.8	65.2	63.7
	Alt-2	46	1	70.3	79.3

For the PXR LBD structures used in this study, the calculated size (number of alpha spheres) of the LBP, AF-2 groove, and the alternative pockets (Alt-1, Alt-2) are listed, along with the calculated propensity for ligand binding (PLB) at these sites. For each pocket, the top-ranked docking scores of nelfinavir (NFV) and M8 are provided. n.d., not determined.

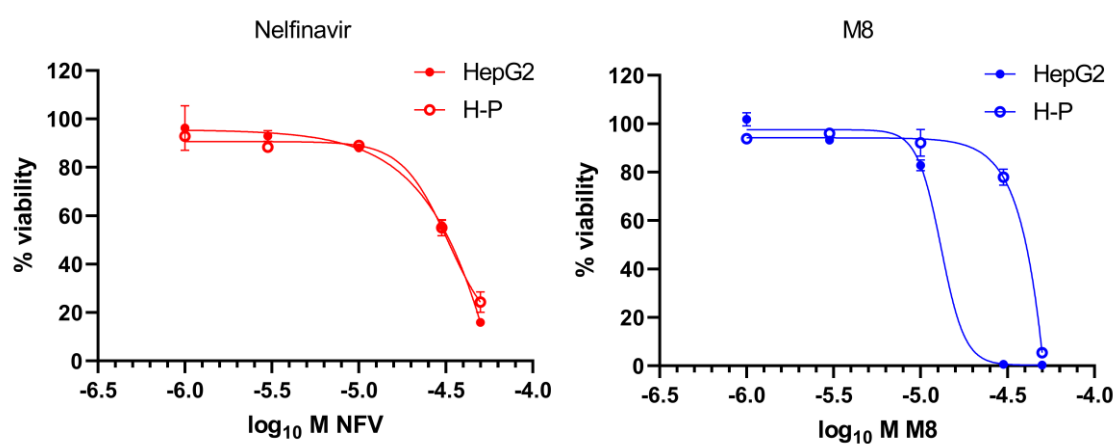
Supplemental Table S3. Number of docking poses per cluster and their ranking according to the docking score within the set of 100 docking conformations

Cluster	Nelfinavir		M8	
	Cluster Size	Docking Poses	Cluster Size	Docking Poses
1	8	1,2,4,5,6,8,16,51	4	1,2,5,11
2	1	3	4	3,4,24,27
3	4	7,9,13,14	3	6,12,42
4	1	10	4	7,9,21,32
			3	8,16,73
			1	10

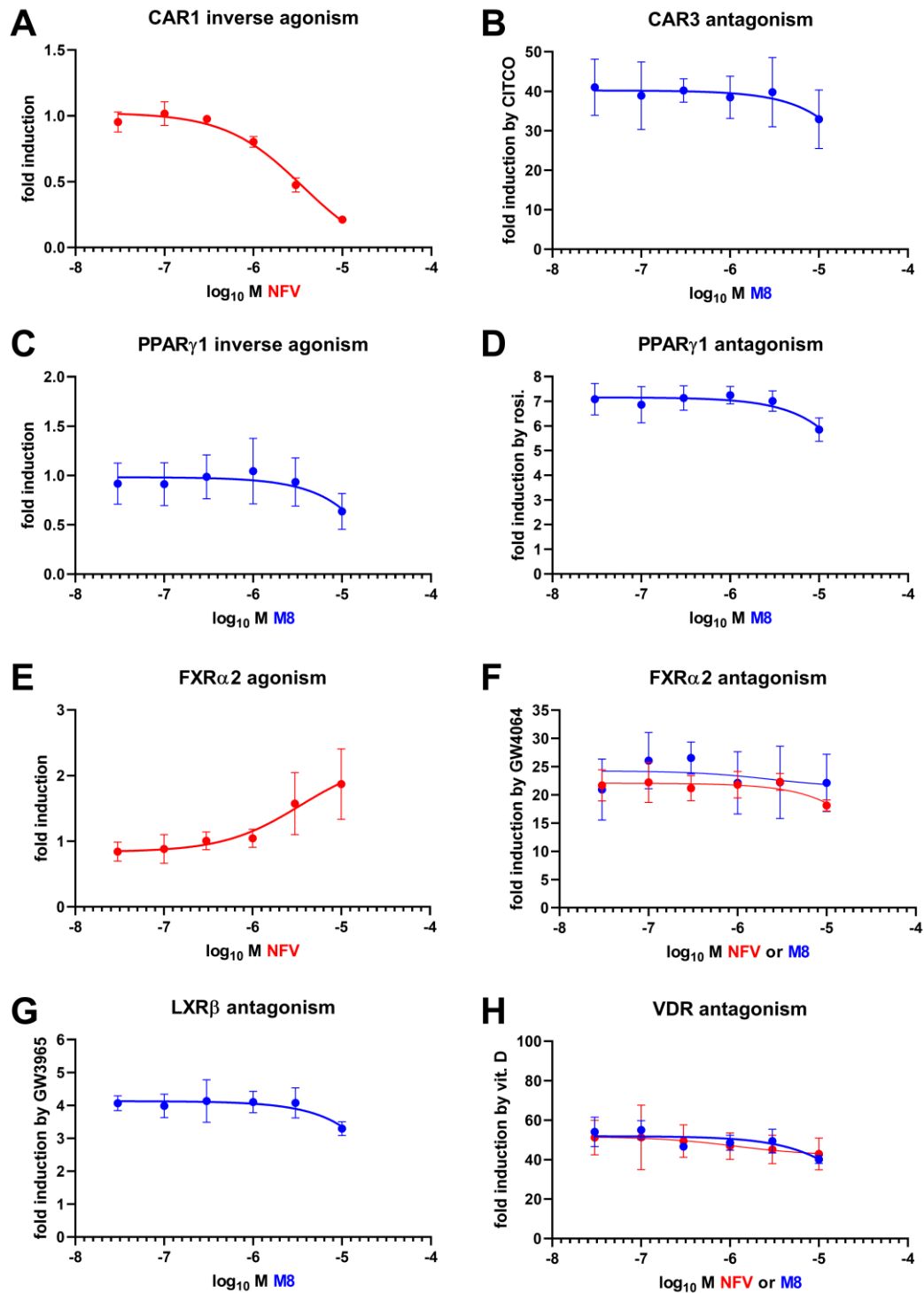
Supplemental Table S4 Rifampin EC₅₀ with increasing doses of nelfinavir and M8

NFV [μM]	Rifampin		M8 [μM]	Rifampin	
	EC ₅₀ [μM]	95% CI [μM]		EC ₅₀ [μM]	95% CI [μM]
0	2.0	1.2 - 3.3	0	1.6	0.97 - 2.7
3	5.4	3.4 – 8.8	3	2.1	1.1 - 4.1
10	19.7	6.9 - 158	10	5.9	5.4 - ???

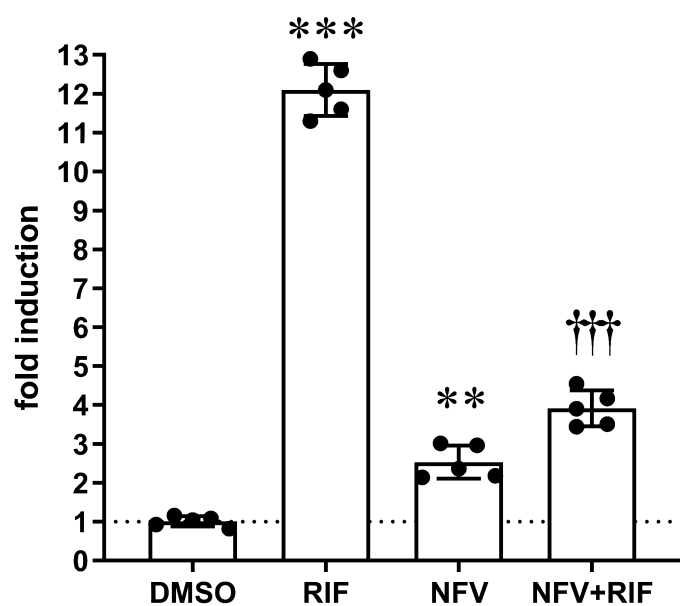
???, not computable by GraphPad Prism



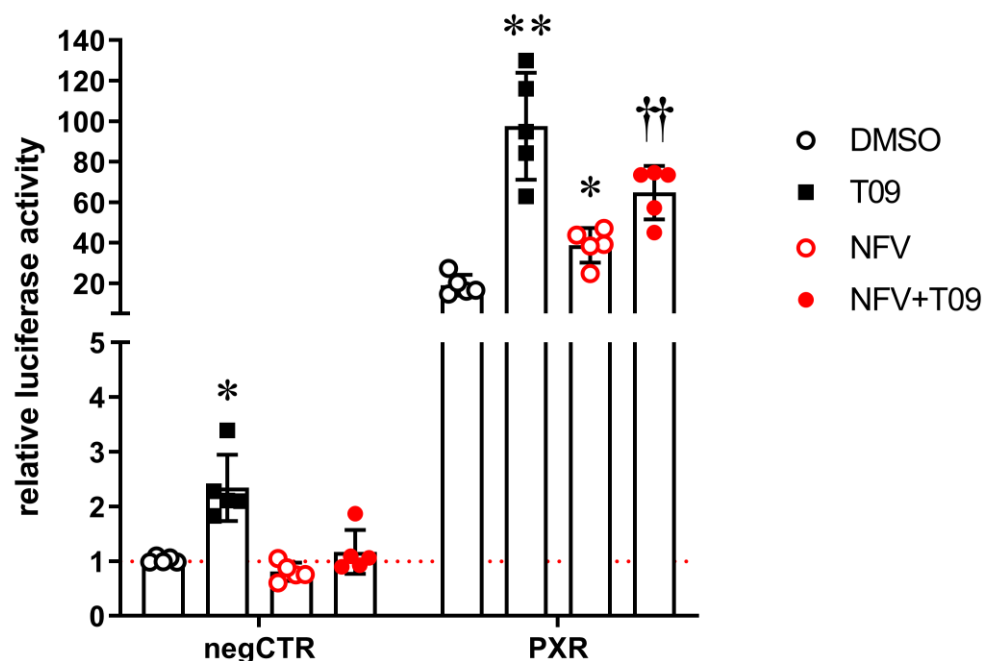
Supplemental Fig. S1. Cell toxicity of nelfinavir and M8. HepG2 and H-P cells were treated with increasing concentrations of nelfinavir or M8 metabolite for 24 h. Means \pm SD ($N=2$) are shown.



Supplemental Fig. S2. Concentration response analyses of the effects of nelfinavir and/or M8 on nuclear receptors beside PXR. HepG2 cells were co-transfected with expression plasmids encoding human CAR1 (A), CAR3 (B), PPAR γ 1 (C, D), FXR α 2 (E, F), LXR β (G) or VDR (H) and the corresponding reporter gene plasmids (see Materials and Methods). Transfected cells were treated with increasing concentrations of nelfinavir (NFV) or M8, alone (A, C, E) or in combination with respective receptor agonists (B, D, F-H), as indicated. Mean fold induction \pm SD ($n=3$) by the respective treatment is shown, with respect to the normalized reporter activity of cells treated with vehicle DMSO only, which was designated as 1. Non-linear fit of dose response was executed as described in Materials and Methods. rosi., rosiglitazone; vit. D, 1 α ,25-dihydroxyvitamin D3.



Supplemental Fig. S3. Effect of nelfinavir on the GAL4-PXR-LBD fusion protein. HepG2 cells were transfected with expression plasmid encoding GAL4-DBD/PXR-LBD(108-434) fusion protein. Transfected cells were treated with 0.1% DMSO or 10 μ M nelfinavir (NFV) in the absence or presence of 10 μ M rifampin (RIF) for 24h. Data are presented as scatter plots with means (columns) \pm S.D. ($n=5$) of normalized luciferase activity of co-transfected pGL3-G5, relative to the activity of cells treated with vehicle DMSO only. Differences to respective treatments with DMSO (asterisks, exclusively for single compound treatments) or rifampin alone (daggers, exclusively for rifampin co-treatment) were analyzed by repeated measures one-way ANOVA with Dunnett's multiple comparisons test or paired t-test, respectively.



Supplemental Fig. S4. Effect of nelfinavir on PXR activation by the high affinity agonist T0901317. HepG2 cells were transfected with empty vector pcDNA3 (negCTR) or expression plasmid encoding human PXR and treated with 0.1% DMSO or 10 μ M nelfinavir (NFV), with or without 1 μ M T0901317 (T09) for 24 h. Data are presented in scatter plots with means (columns) \pm SD ($n=5$) of normalized luciferase activity of co-transfected CYP3A4 reporter, relative to the activity of cells transfected with pcDNA3 and treated with DMSO only. Differences to respective treatments with DMSO (asterisks, exclusively for single compound treatments) or T0901317 alone (daggers, exclusively for T0901317 co-treatments) were analyzed by repeated measures two-way ANOVA with Dunnett's multiple comparisons test. *, $P<0.05$; **, $P<0.01$.